Report No. 1

First Quarterly Progress Report | Covering the Period 1 January to 31 March 1963

NOVEL MICROWAVE FILTER DESIGN TECHNIQUES

Prepared for:

ELECTRONIC COMPONENTS RESEARCH DEPARTMENT
ELECTRONIC PARTS AND MATERIALS DIVISION
MICROWAVE AND ELECTROMECHANICAL BRANCH
U.S. ARMY ELECTRONICS RESEARCH AND DEVELOPMENT LABORATORY
FORT MONMOUTH, NEW JERSEY

CONTRACT DA 36-039-AMC-00084(E)

By: G. L. Matthaei E. G. Cristal L. A. Robinson B. M. Schiffman

STANFORD RESEARCH INSTITUTE

MENLO PARK, CALIFORNIA

SRI

STANFORD RESEARCH INSTITUTE
MENLO PARK, CALIFORNIA

April 1963

Report No. 1

First Quarterly Progress Report | Covering the Period 1 January to 31 March 1963

NOVEL MICROWAVE FILTER DESIGN TECHNIQUES

Prepared for:

ELECTRONIC COMPONENTS RESEARCH DEPARTMENT
ELECTRONIC PARTS AND MATERIALS DIVISION
MICROWAVE AND ELECTROMECHANICAL BRANCH
U.S. ARMY ELECTRONICS RESEARCH AND DEVELOPMENT LABORATORY
FORT MONMOUTH, NEW JERSEY CONTRACT DA 36-039-AMC-00084(E)

By: G. L. Matthaei E. G. Cristal L. A. Robinson B. M. Schiffman

SRI Project No. 4344

Approved:

D. R. SCHEUCH, DIRECTOR ELECTRONICS AND RADIO SCIENCES DIVISION

Copy No. 20

ABSTRACT

In Sec. II the results of a mathematical study of a proposed multiplexer design technique are presented. Using this technique a separate channel unit is used for each channel that is to be separated out. Each channel unit consists of a band-pass filter and a band-stop filter. At the frequencies to be separated by a given channel unit, the band-pass filter will pass the signal to be separated, while the band-stop filter blocks any energy from escaping down the main transmission line. At frequencies outside the band to be separated, the energy flows through the channel unit without attenuation. It is shown that such units can be designed to have a constant-resistance input impedance, hence, in theory, any number of units can be cascaded without interaction effects. Each channel unit has properties similar to those of a directional filter, but such channel units should be much easier to design and tune than are equivalent multi-resonator directional filters.

In Sec. III, techniques for the design of magnetically tunable band-stop filters using ferrimagnetic garnet resonators (such as yttrium-iron-garnet spheres) are presented. Design for prescribed response, starting from a low-pass lumped-element prototype filter is outlined. The filter structure consists of a strip line or waveguide with garnet spheres mounted at intervals of approximately a quarter wavelength or three quarters wavelength, at the center of the tuning range. Tuning is achieved by varying a biasing magnetic field. Techniques for enhancing the coupling to the garnet-sphere resonators are discussed, and the results of experiments to verify the theory are presented. The band-stop filter techniques are shown to also provide a very simple means for measuring the ferrimagnetic resonance linewidth ΔH of garnet spheres.

In Sec. IV a study of the use of varactor diodes for tuning transmission line resonators for a proposed form of band-pass filter phase shifter is discussed. One of the problems encountered is that unless special precautions are taken the unloaded Q of the resonator will vary greatly as the resonator is tuned. Means for avoiding this difficulty are outlined.

In Sec. V the experimental results obtained from a trial interdigital filter with capacitively loaded resonators are presented. Design theory for such filters was presented previously, and the measured results were in good agreement with the theory. This filter had a bandwidth of roughly an octave centered at about 1.5 Gc. The interesting features of this filter are its very small size and its very broad upper stop band. The filter was without additional pass bands or spurious responses up to the second pass band, which was centered at 6.7 Gc.

CONTENTS

ILLUSTRATIONS

ILLUSTRATIONS

TABLES

PURPOSE OF THE CONTRACT

This contract continues the work of Contract DA 36-039 SC-87398 to develop improved design techniques for waveguide, strip-line, and coaxial-line microwave filters and related microwave components.

CONFERENCES AND TECHNICAL PAPERS

CONFERENCES

On 11 January 1963 Dr. G. L. Matthaei of SRI visited Ft. Monmouth and discussed the course of this research work with Mr. W. P. Dattilo of the U.S. Army Electronics Research and Development Laboratory.

TECHNICAL PAPERS

Leo Young and M. B. Schiffman, "A Useful High-Pass Filter Design," *The Microwave Journal*, Vol. 6, pp. 78-80 (February 1963).

G. L. Matthaei, "Some Microwave Filter Design Concepts and Their Application to the design of Microwave Devices," a talk presented at the 20 March 1963 meeting of the Philadelphia Chapter of the PTGMTT, and also presented at the 21 March 1963 meeting of the Washington, D. C. Chapter of the PGTMTT.

Leo Young, "The Analytical Equivalence of TEM-Mode Directional Couplers and Transmission-Line Stepped-Impedance Filters," *Proc. IEE* (London) Vol. 110, pp. 275-281 (February 1963).

I INTRODUCTION

A problem that occurs quite frequently in complex microwave systems is that of designing multiplexers to break up a large band of signals into a number of separate channels, with the signals in the various channels well isolated from each other. In the past, directional filters have appeared attractive for this purpose because, in theory, they have a constant-resistance input impedance; thus it should be possible to cascade a large number of directional channel-separation filters without harmful interaction effects. However, in practice, directional filters have not proved as desirable as might be expected because the mechanically simple types are difficult to design and tune when many resonators per filter are involved, while the types that are easy to tune are physically complicated (they involve two filters and two hybrid junctions per channel-separation unit). In Sec. II of this report, a mathematical analysis is made of the potentialities of another form of channel-separation unit, which should be easy to tune, which need not be physically complicated, and which can (in theory) be designed to have the constant-resistance properties (or nearly constant-resistance properties) of a directional filter.

In previous work on Contract DA 36-039 SC-87398, considerable study has been made of design techniques for magnetically tunable filters employing ferrimagnetic garnet resonators. In Sec. III of this report, the results of additional work of this sort is presented. Most of the past work has dealt with band-pass filters, while the work discussed in Sec. III treats band-stop filters such as would be desirable for the elimination of a single interfering signal. This work has also led to an unusually simple means for measuring the resonance linewidth ΔH of a ferrimagnetic material. This is of importance in evaluating the quality of garnet spheres for use in magnetically tunable filters.

On Contract DA 36-039 SC-74862, a number of different possible techniques for electronic tuning of microwave filters were evaluated including tuning by use of ferrites, electronically tunable up-converters, and tuning of resonators by use of varactor diodes as voltage-controlled capacitors.

The varactor diode approach was shown to be impractical for typical microwave filter tuning applications because of the relatively low Q of presently available diodes. However, in Sec. IV of this report, the design of resonators tuned by varactor diodes is evaluated for use where very limited tuning range is required. A proposed case of this type is a band-pass filter type of phase shifter. One of the problems treated is the problem of design of the resonator so as to give a reasonably constant unloaded Q as the tuning of the resonator is varied.

In the Final Report for Contract DA 36-039 SC-87398, design theory was presented for interdigital filters having capacitive loading on the resonators. Such filters were predicted to have advantages of very small size and the capability of having a very broad stop band above the pass band. In Sec. V of the present report, the experimental results obtained from a trial design are presented.

II MULTIPLEXERS

A. GENERAL

This section discusses the design of multiplexers that have narrow bandwidth transmission channels separated from adjacent channels by guard bands. A schematic representation of a multiplexer of a particular design that is being investigated is shown in Fig. II-1. The band-pass and band-stop filters adjacent to each other in the figure are designed to work conjunctly. In a frequency interval in which Channel 1, for example, is to receive energy, the band-stop Filter 1 is designed to stop transmission of the signal energy, thus isolating the other channels. At the same time the band-pass filter comprising Channel 1 is designed to accept the signal energy. At frequencies outside of the pass band of Channel 1, the band-pass and band-stop filters are designed so that their residual reactances tend to cancel each other. This minimizes interchannel interference and the resulting energy reflections.

This method of design can analytically be shown to give unity VSWR at the multiplexer input at all frequencies if one uses maximally flat, singly terminated filters for both the band-pass and band-stop filters of the multiplexer. A requirement on these filters, however, is that

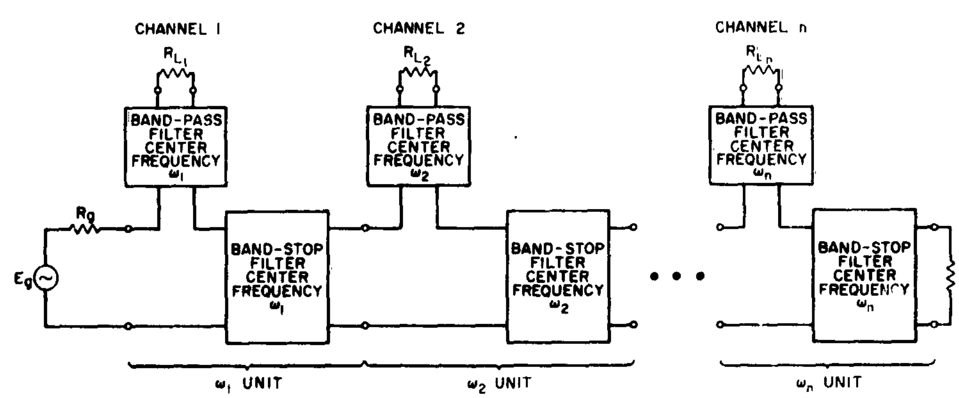

FIG. II-1 SCHEMATIC REPRESENTATION OF A MULTIPLEXER OF A PARTICULAR DESIGN any pair acting conjunctly have the same number of reactive elements. In that the multiplexer of Fig. II-1 can theoretically give unity VSWR at all frequencies, it is similar in its behavior to multiplexers that use multi-resonator directional filters.[1*] However, the design of Fig. II-1 offers the practical advantage that it should be considerably easier to tune than multiplexers using multi-resonator directional filters.

A singly terminated low-pass filter prototype is shown in Fig. II-2. It is designed on the premise that it is to be driven by an infinite-impedance current generator. The singly terminated filter has the property that

$$20 \log_{10} \left| \frac{I_g}{I_L} \right| = 10 \log_{10} \frac{R_0'}{\mathrm{Re}[Z_{in}']} \quad . \qquad \text{(II-1)}$$

Therefore, the transmission response has the same type of behavior as the real part of the input impedance.

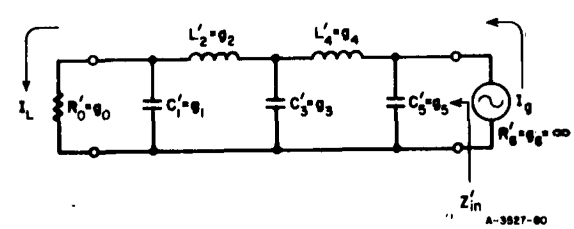

FIG. II-2 LOW-PASS LUMPED-ELEMENT PROTOTYPE FILTER DRIVEN BY AN INFINITE-IMPEDANCE CURRENT GENERATOR

A maximally flat singly terminated low-pass filter having a 3 db cutoff frequency at $\omega' = \omega_1'$ has a normalized real part of

$$\frac{\mathrm{Re}[Z_{in}'(\omega')]}{R_0'} = \frac{1}{1 + \left(\dfrac{\omega'}{\omega_1'}\right)^{2n}} \quad , \qquad \text{(II-2)}$$

where n is the number of reactive elements in the filter. We will use Eq. (II-2) to demonstrate that use of maximally flat, singly terminated

* References for each section are grouped at the end of the section.

filters as prototypes for the band-pass and band-stop filters of the multiplexer of Fig. II-1 can result in a multiplexer design that, theoretically, has unity VSWR at all frequencies.

B. MULTIPLEXER DESIGN USING SINGLY TERMINATED FILTER PROTOTYPES

A suitable transformation for obtaining a high-pass filter design from a low-pass filter design in the case of lumped element filters is

$$\frac{\omega'}{\omega_1'} \rightarrow \frac{1}{\left(\dfrac{\omega'}{\omega_1'}\right)} \quad . \qquad \text{(II-3)}$$

This transformation corresponds to replacing in the low-pass filter all inductors of value L' by capacitors of value $1/L'$; and all capacitors of value C' by inductors of value $1/C'$. Substituting Eq. (II-3) into Eq. (II-2) gives, for the $\mathrm{Re}[Z_{in}']/R_0'$ of the high-pass filter, the expression

$$\left\{\frac{\mathrm{Re}\,[Z_{in}']}{R_0'}\right\}_{\text{high-pass}} = \frac{\left(\dfrac{\omega'}{\omega_1'}\right)^{2n}}{1 + \left(\dfrac{\omega'}{\omega_1'}\right)^{2n}} \quad . \qquad \text{(II-4)}$$

If the low-pass and high-pass filters are arranged in series, we have

$$\left\{\frac{\mathrm{Re}[Z_{in}']}{R_0'}\right\}_{\text{low-pass}} + \left\{\frac{\mathrm{Re}[Z_{in}']}{R_0'}\right\}_{\text{high-pass}} = 1 \quad . \qquad \text{(II-5)}$$

Using Bode's integral relationship relating real and imaginary parts of minimum reactance networks[2] it can be shown that when Eq. (II-5) holds,

$$\left\{\frac{\mathrm{Im}\,[Z_{in}']}{R_0'}\right\}_{\text{low-pass}} + \left\{\frac{\mathrm{Im}\,[Z_{in}']}{R_0'}\right\}_{\text{high-pass}} = 0 \quad . \qquad \text{(II-6)}$$

Figure II-3(a) shows the proper physical arrangement of the prototype low-pass and high-pass filters to realize Eqs. (II-5) and (II-6). In Fig. II-3(a), Z_{AC} represents the input impedance of the low-pass filter and is given in normalized form by Eq. (II-2); Z_{CB} represents the input impedance of the high-pass filter and is given in normalized form by Eq. (II-4); Z_{AB} is the sum of Z_{AC} and Z_{CB}, and by Eq. (II-5) is unity (normalized with respect to the load resistor) at all frequencies. Thus, by selecting the generator resistance equal to the load resistance, the VSWR seen at the terminals A-B in Fig. II-3(a) is unity at all frequencies. The low-pass and high-pass filter attenuations corresponding to the circuit of Fig. II-3(a) are sketched in Fig. II-3(b).

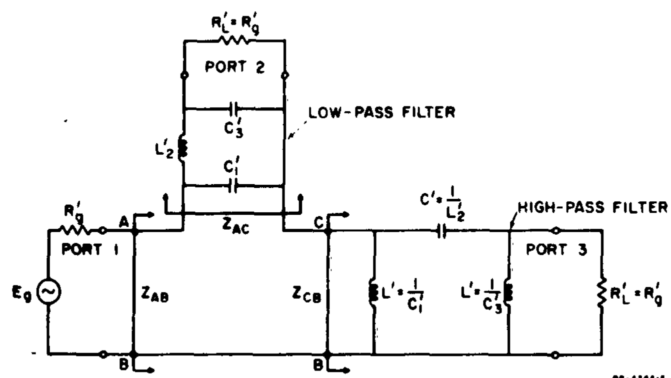

FIG. II-3(a) SCHEMATIC SHOWING THE ARRANGEMENT OF THE PROTOTYPE LOW-PASS AND PROTOTYPE HIGH-PASS FILTER

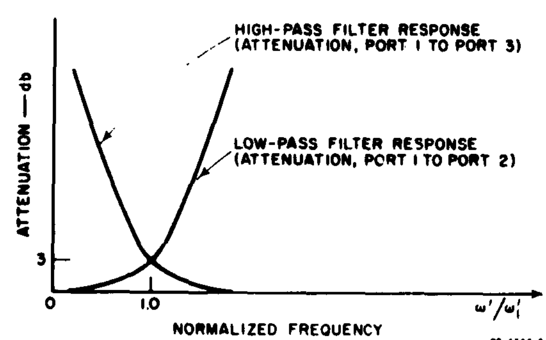

FIG. II-3(b) CORRESPONDING FILTER RESPONSES OF THE CIRCUIT OF (a)

Next to be shown is that the multiplexer of Fig. II-1 may be realized from the basic prototype circuit given in Fig. II-3(a). To demonstrate this, the low-pass and high-pass filter of Fig. II-3(a) are converted to band-pass and band-stop filters, respectively. The conversion is accomplished mathematically through the frequency transformation

$$\omega' = \frac{\omega_1'}{w}\left(\frac{\omega}{\omega_j} - \frac{\omega_j}{\omega}\right) , \tag{II-7}$$

where

ω' is the frequency variable of the prototype filters,

ω is the frequency variable of the band-pass and band-stop filters,

ω_j is the center frequency of the band-pass and band-stop filters for channel j,

w is the fractional bandwidth of the band-pass and band-stop filters, and is defined by the equation

$$w = \frac{\omega_b - \omega_a}{\omega_j} , \tag{II-8}$$

where ω_b and ω_a are the frequencies at which the $\omega' = \omega_1'$.

Physically, the transformation (II-7) corresponds to replacing in the low-pass and high-pass filters:

(1) All inductors of value L' by a series combination of inductor and capacitor of value L and C where

$$\left.\begin{aligned} L &= \frac{wL'}{\omega_1'\omega_j} \\ C &= \frac{\omega_1'}{w\omega_j L'} \end{aligned}\right\} , \tag{II-9}$$

(2) All capacitors of value C' by a parallel combination of capacitor and inductor of value C'' and L'' where

$$\left.\begin{aligned} C'' &= \frac{wC'}{\omega_1' \omega_j} \\ L'' &= \frac{\omega_1'}{w\omega_j C'} \end{aligned}\right\} \quad . \qquad \text{(II-10)}$$

As a result of the transformation (II-7), the circuit of Fig. II-3(a) is transformed into that of Fig. II-4(a) and the response of the circuit of Fig. II-3(a) is transformed into that of Fig. II-4(b). Note that the identities, Eqs. (II-5) and (II-6), are not affected by the transformation, so that the impedance Z_{AB} remains

$$Z_{AB} = R_g$$

at all frequencies. Since the band-pass and band-stop filters act conjunctly to give a constant input resistance independent of frequency, the terminating resistance of the band-stop filter at Port 3 may be replaced by another pair of band-pass and band-stop filters acting conjunctly, without affecting the performance of the preceding pair of filters. The only requirement is that the input resistance of each pair must equal the proper terminating resistance of the preceding band-stop filter. By spacing the center frequencies of each pair of filters, the multiplexer response of Fig. II-5 is obtained and a multiplexer of the type given in Fig. II-1 is achieved.

Chebyshev singly terminated filters may also be used for the various band-pass and band-stop filters of the multiplexer. However, these filters do not have the desirable property of Eq. (II-5). This means that residual reactance will appear throughout the pass band of the multiplexer, resulting in inter-channel interference and non-optimum transfer of signal energy between source and load. On the other hand, the Chebyshev filter has a greater rate of attenuation outside the pass band than the maximally flat filter of the same number of elements. Therefore, for some purposes, it may be desirable to use Chebyshev filters, if the residual reactance can be tolerated for the particular application of the multiplexer.

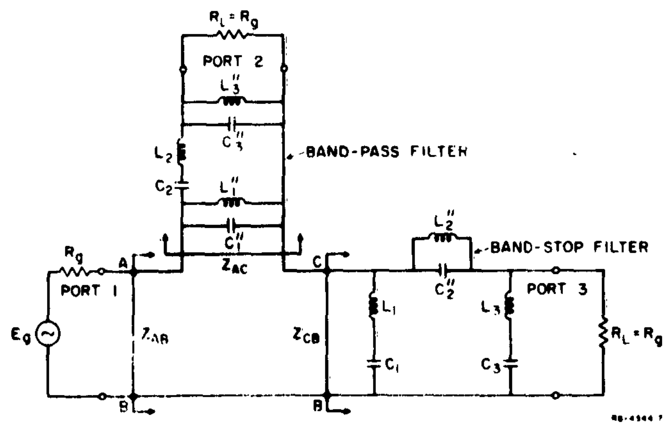

FIG. II-4(a) SCHEMATIC OF THE BAND-PASS AND BAND-STOP FILTERS DERIVED FROM THE PROTOTYPE FILTERS OF FIG. II-3(a) BY TRANSFORMATION (II-7)

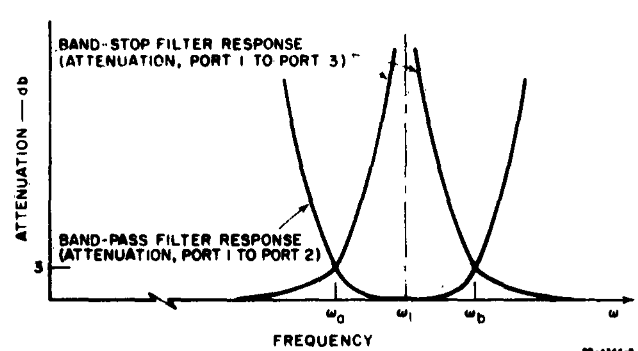

FIG. II-4(b) CORRESPONDING FILTER RESPONSES TO THE CIRCUIT OF (a)

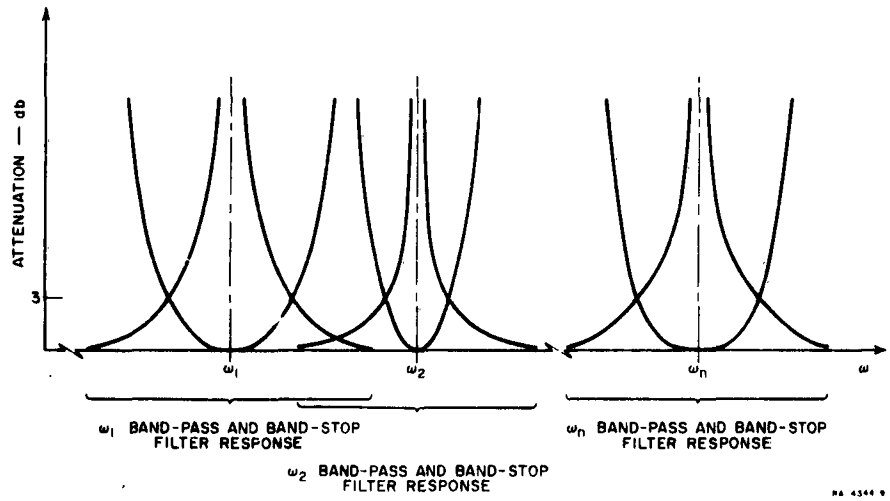

FIG. II-5 HYPOTHETICAL IDEALIZED RESPONSE OF THE MULTIPLEXER OF FIG. II-1 CONSTRUCTED FROM MAXIMALLY FLAT SINGLY TERMINATED BAND-PASS AND BAND-STOP FILTERS

C. MULTIPLEXER DESIGN USING OTHER FILTER PROTOTYPES

In some applications, it may be desirable to design the band-stop filters with fewer resonators than are used in the band-pass filters. If this could be satisfactorily accomplished, there would result a considerable simplification in the tuning and a reduction in size and weight of the multiplexer. A procedure for such a design is described in this part. It is based upon using singly terminated prototype filters for the band-pass filters and doubly terminated prototype filters (*i.e.*, filters that are designed to be driven by sources having finite, non-zero impedances) for the band-stop filters.

In the following discussion, we use only low-pass and high-pass filters in the examples in order to simplify the design procedure and the graphs of the worked examples. However, the resulting filter designs and responses may be converted into the proper band-pass and band-stop filters and responses by suitable transformations, such as Eq. (II-7). In the following discussion the low-pass, high-pass filter configuration of Fig. II-3(a) will be referred to as a prototype *channel unit* of the multiplexer of Fig. II-1.

The design procedure is based on the fact that outside the pass band of the low-pass filter, Z_{AC} [See Fig. II-3(a)] tends to look capacitive. In fact, an asymptotic series for the Im $[Z_{AC}(\omega)]$ is

$$\left| \mathrm{Im}\,[Z_{AA}(\omega)] \right| = \frac{1}{\omega A_1} + \frac{1}{(\omega A_3)^3} + \frac{1}{(\omega A_5)^5} + \ldots \qquad \text{(II-11)}$$

If the value of A_1 can be discovered in a truncated asymptotic series*, we can identify this constant with an equivalent capacitor, C_{eq}, which is in series with the high-pass filter. Once C_{eq} is known, a doubly terminated high-pass filter whose leading element is C_{eq} can be designed. By selecting the proper filter design prototype, the residual off-band VSWR can be limited to less than any desired value.

Assuming that this can be done and that the off-band VSWR is sufficiently small, other channel units may be cascaded with the first channel unit with only small interaction. The number of channel units that can be cascaded will depend on the extent to which the residual VSWR's of the units build up, and upon the performance required for the particular application of the multiplexer. We point out that this design method focuses attention upon minimizing the residual VSWR in the off-band region and does not directly consider the annulling of the reactance of the low-pass filter in its pass band. Therefore, the method may or may not adversely affect the pass-band attenuation of the low-pass filter.

A computer study of the prototype of Fig. II-3(a) was made in which the number of elements of the high-pass prototype filter was increased from one element to two, to three, and so on, until the low-pass prototype filter and the high-pass prototype filter had the same number of elements. In the study, the low-pass filter was either a four-element maximally flat, or a 0.5-db ripple Chebyshev singly terminated filter. The high-pass filters were designed on the doubly terminated basis as described before. The results of the computer study are given in Figs. II-6, II-7, II-8, and II-9.

Figure II-6 shows the channel unit VSWR for cases in which the low-pass filter is a four-element maximally flat filter, designed on the

* If the asymptotic series of Eq. (II-11) is not truncated, then $A_1 = C_{eq} = C_1'$.

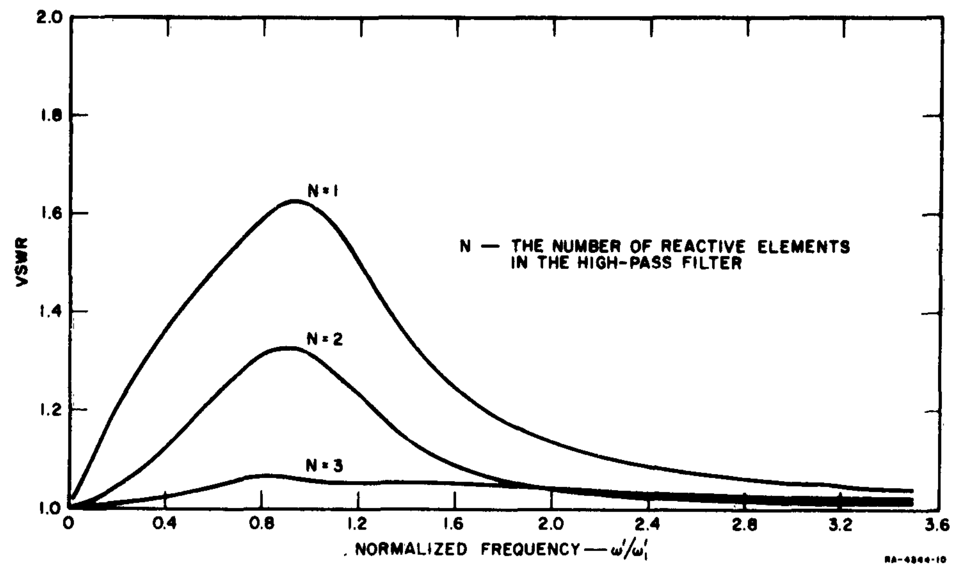

FIG. II-6 VSWR OF THE PROTOTYPE UNIT USING MAXIMALLY FLAT FILTER PROTOTYPES

singly terminated basis. The low-pass filter has a 3-db cutoff frequency of $\omega' = \omega_1'$ The VSWR is computed from

$$r = \frac{\left|Z_{AB} + R_g\right| + \left|Z_{AB} - R_g\right|}{\left|Z_{AB} + R_g\right| - \left|Z_{AB} - R_g\right|} \quad . \qquad \text{(II-12)}$$

The symbol N in Fig. II-6 represents the number of reactive elements seen when viewing the high-pass filter at the terminals C-B of Fig. II-3(a). We note again, however, that the high-pass filter is designed from a doubly terminated prototype of $(N + 1)$ reactive elements, wherein C_{eq} is the leading element of the $(N + 1)$-element high-pass filter. The case $N = 4$ is not shown in Fig. II-4 because it has previously been shown that, for maximally flat filters, when the low-pass and high-pass filters have the same number of elements, unity input VSWR is theoretically obtained at all frequencies.

The corresponding cases using a four-element, 0.5 db ripple Chebyshev singly terminated prototype low-pass filter are given in Fig. II-7. The high-pass filters had one, two, and four reactive elements. The filters having two and four reactive elements are designed from 0.1 db ripple

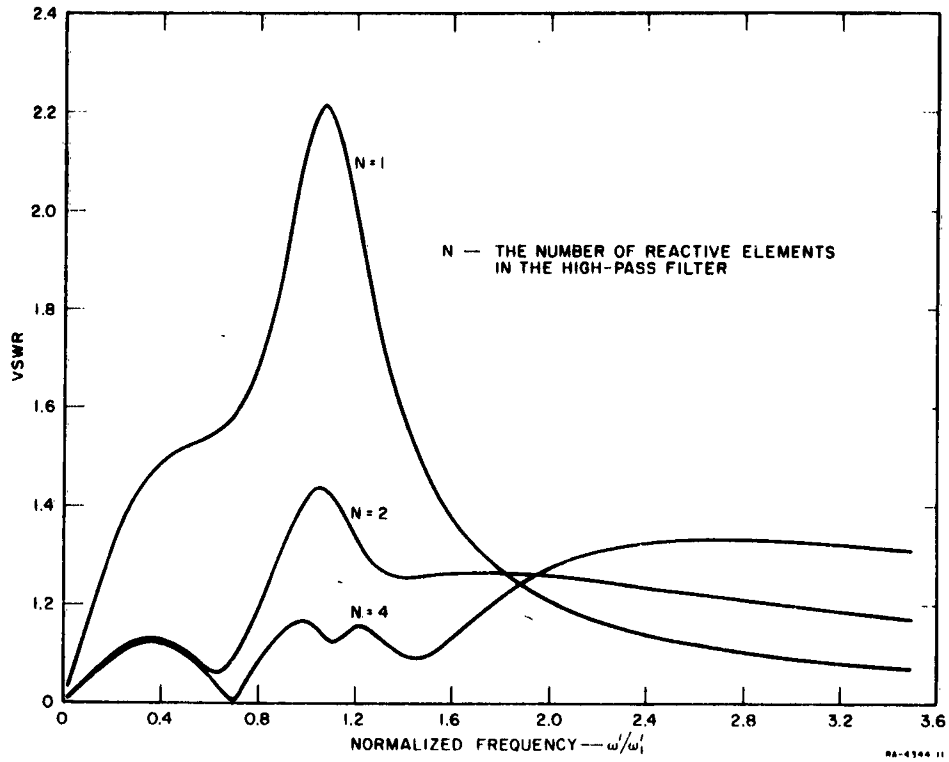

FIG. II-7 VSWR OF THE PROTOTYPE UNIT USING CHEBYSHEV FILTER PROTOTYPES

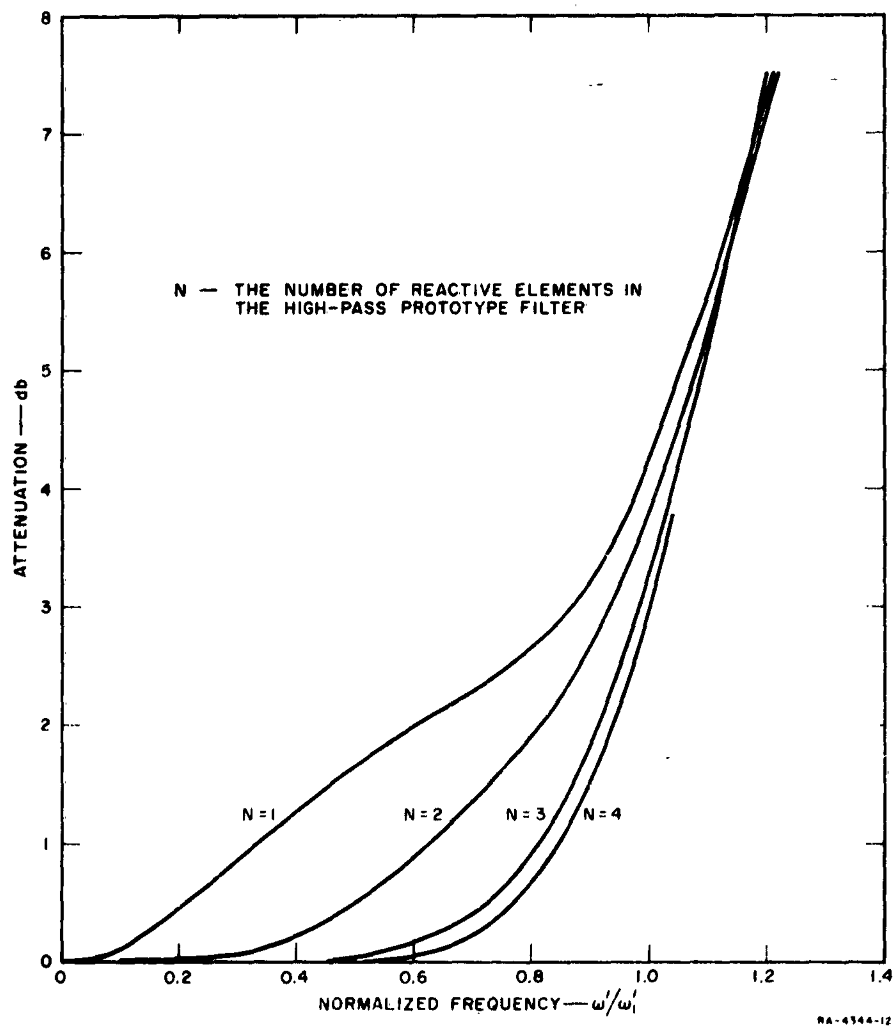

FIG. II-8 PASS-BAND ATTENUATION OF THE LOW-PASS FILTER OF THE PROTOTYPE UNIT, USING MAXIMALLY FLAT FILTER PROTOTYPES

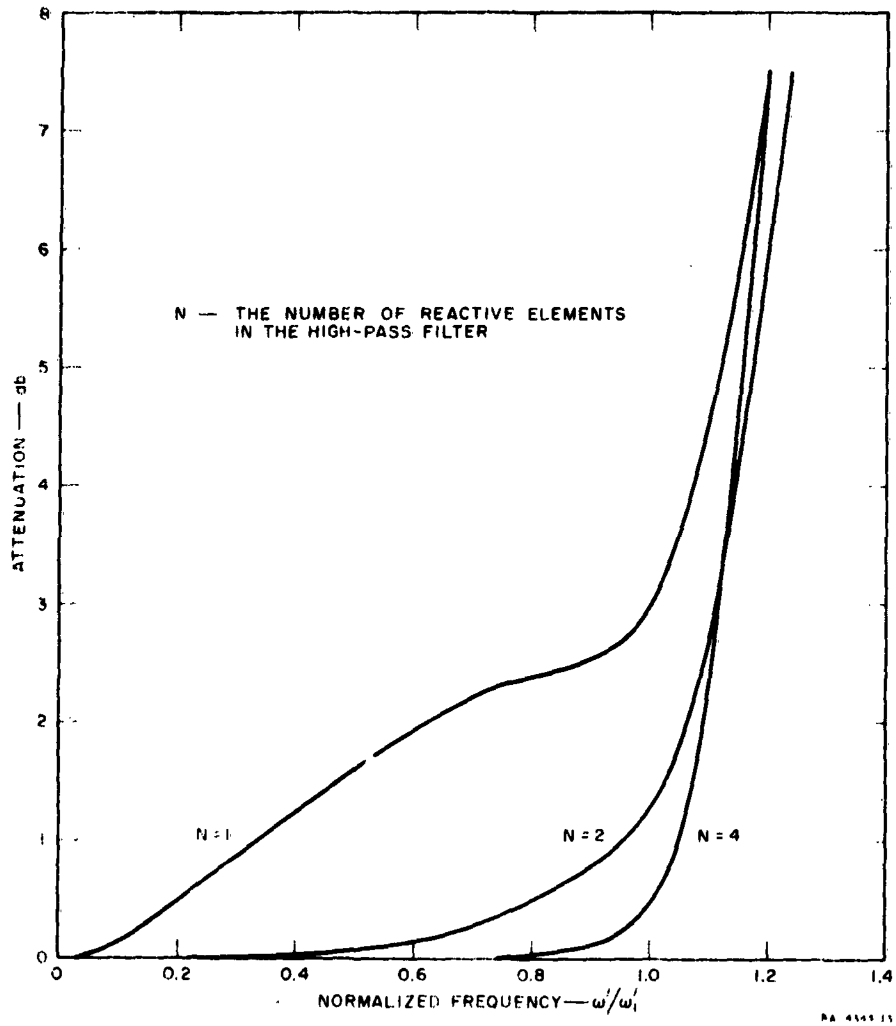

FIG. II-9 PASS-BAND ATTENUATION OF THE LOW-PASS FILTER OF THE PROTOTYPE UNIT, USING CHEBYSHEV FILTER PROTOTYPES doubly terminated Chebyshev prototypes. The $N = 1$ filter is a special case in which the value of the inductive element of the high-pass filter was chosen numerically equal to C_{eq}. In this instance it can be shown that, for $L = C_{eq}$,

$$Z_{AB}(\omega') = \frac{1}{1 + \left(\frac{1}{\omega' L}\right)^2} + j\left\{\frac{\omega' L}{1 + (\omega' L)^2} - \frac{1}{\omega' C_{eq}}\right\} \quad . \tag{II-13}$$

As ω' increases, the $\mathrm{Re}[Z_{AB}]$ approaches unity and the $\mathrm{Im}[Z_{AB}]$ approaches zero.

Comparing Figs. II-6 and II-7 shows that designs using maximally flat filters offer better over-all VSWR's over designs using Chebyshev filters, although the off-band VSWR when using Chebyshev filters could be reduced by designing from smaller ripple high-pass prototypes.

Figures II-8 and II-9 give the pass-band attenuation of the maximally flat and Chebyshev cases, respectively. The designs using Chebyshev filters are seen to cover the pass-band with smaller attenuation and also have a greater rate of attenuation after cutoff than the corresponding maximally flat cases.

In the previous paragraphs a design method for the synthesis of the basic channel unit of the multiplexer of Fig. II-1 (*i.e.*, a band-pass and band-stop filter acting conjunctly) was given and worked examples presented. The method depended on estimating the off-band reactance of the low-pass prototype filter and approximating this reactance by a lumped capacitance, which was denoted as C_{eq}. It has been found that suitable approximations for C_{eq} are given by

$$C_{eq} = C_1(1 + \Delta) \quad , \tag{II-14}$$

where C_1 is the capacitor at the A-C terminals [Fig. II-3(a)] of the low-pass filter prototype; and Δ is a small number that typically ranges as

$$0.01 < \Delta < 0.15 \quad . \tag{II-15}$$

No rule is stated for determining Δ; however, there are these guide-lines:

(1) The value of Δ used for a Chebyshev filter of *n* elements will be less than for a maximally flat filter of *n* elements.

(2) For both Chebyshev and maximally flat filters, Δ decreases as the number of elements in the filters increase.

D. EXPERIMENTAL WORK

The structure of Fig. II-10(a) is presently being investigated to determine its merits as a multiplexer prototype unit consisting of a band-pass and band-stop filter acting conjunctly. The approximate equivalent circuit for the structure of Fig. II-10(a) is given in Fig. II-10(b). Figure II-10(a) represents a single cavity band-pass filter that is coupled to the main waveguide by a rectangular slot in the broad wall of the waveguide, and a single cavity resonator that is coupled to the waveguide by a longitudinal slot in the narrow wall. The slots are intentionally close together (in terms of operating wavelength) because the purpose of the experimental work is to determine whether two filters oriented in this manner can be sufficiently de-coupled to perform satisfactorily in the pass band and also give sufficiently small off-band VSWR to permit cascading several similar structures.

It is anticipated that the two coupling slots will be mutually coupled by the evanescent fields about the slots, but it is hoped that the particular physical placement of the slots will minimize this effect. Should the configuration of Fig. II-10(a) prove satisfactory, considerable saving in length of the multiplexer will result.

REFERENCES

1. G. L. Matthaei, L. Young and E. M. T. Jones, *Design of Microwave Filters, Impedance-Matching Networks, and Coupling Structures*, a book prepared on SRI Project 3527, Contract DA 36-039 SC-87398, Stanford Research Institute, Menlo Park, California (January 1963), Vol. II, pp. 958-959.

2. H. Bode, *Network Analysis and Feedback Amplifier Design*, (D. Van Nostrand Company, Inc., New York, New York 1945), p. 335.

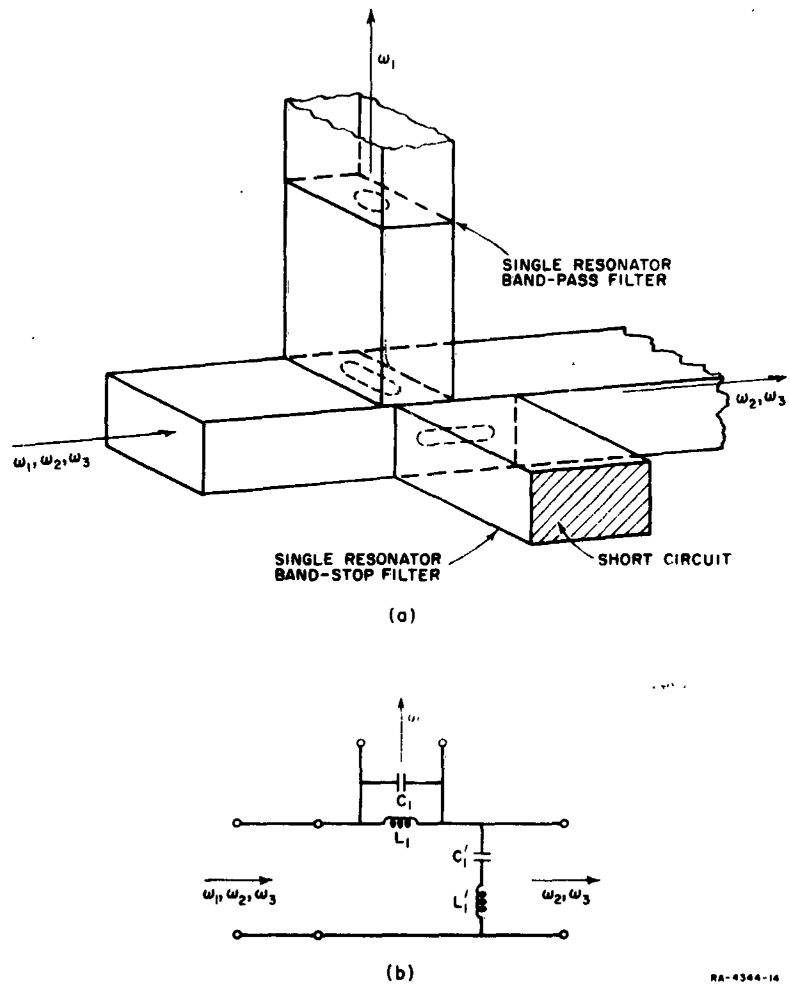

FIG. 11-10 MULTIPLEXER CONFIGURATION UNDER STUDY
(a) Physical arrangement of the single resonator filters
(b) Approximate equivalent circuit

III MAGNETICALLY TUNABLE BAND-STOP FILTERS, AND A SIMPLE TECHNIQUE FOR GARNET LINEWIDTH MEASUREMENT

A. GENERAL

Magnetically tunable filters are of interest for applications where it is desired to blank out an interfering signal, using electronic control to adjust the blanking frequency. One possible application for this type of device is in combination with a swept-frequency superheterodyne receiver. A narrow-band, magnetically tunable band-stop filter could be used to eliminate the image response of such a receiver: As the receiver operating band is swept, the stop band of the filter could also be swept so as continuously to eliminate the image response.

The resonators of the filters under discussion use ferrimagnetic resonance in spheres of such material as single-crystal, yttrium-iron-garnet (YIG).[1*] In YIG resonators, the resonant frequency can be controlled by varying a biasing, dc magnetic field.[1,2] Figure III-1

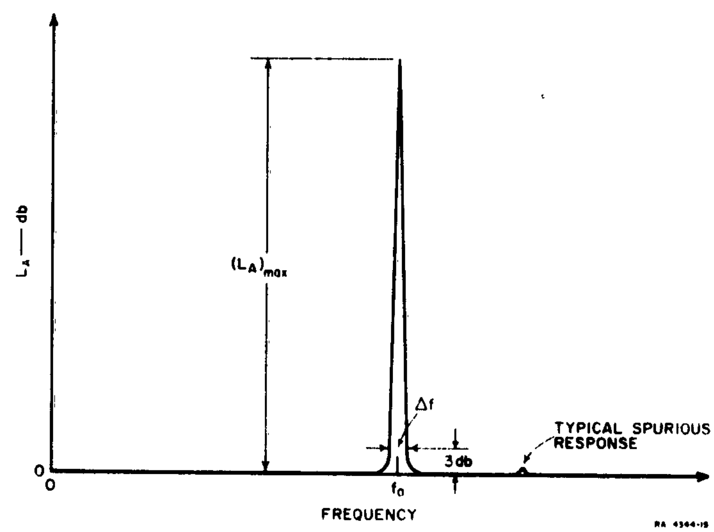

FIG. III-1 DEFINITION OF BAND-STOP FILTER RESPONSE PARAMETERS

* References for Sec. III are grouped at the end of the section.

shows a typical band-stop filter response obtainable using ferrimagnetic resonators. Note that a small spurious response is indicated. Such responses result from higher-order magnetostatic-mode resonances, as occur from non-uniformities in the dc or RF fields within the resonator spheres.

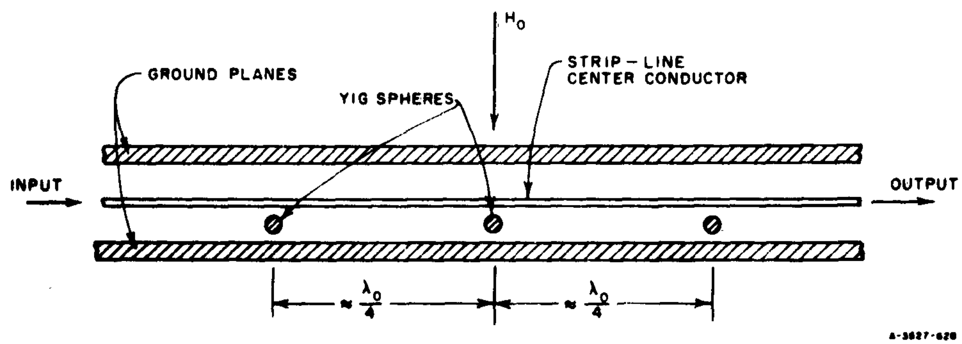

FIG. III-2 A MAGNETICALLY TUNABLE STRIP-LINE BAND-STOP FILTER

Figure III-2 shows one form of strip-line, band-stop filter, which can be tuned by varying the biasing field strength H_0. The filter shown uses three YIG resonators, each of which is magnetically coupled to the strip-line center conductor. Figure III-3(a) shows an equivalent circuit for a ferrimagnetic resonator with its magnetic coupling to the transmission line. In the vicinity of resonance, the circuit in Fig. III-3(a) can be replaced by the circuit shown in Fig. III-3(b). Thus, in the vicinity of resonance, the filter in Fig. III-2 may be viewed as having three anti-resonant circuits connected in series with lines approximately a quarter-wavelength long.

Figure III-4 shows a waveguide version of the filter in Fig. III-2. In this design, the region in which the YIG spheres are located uses reduced height guide in order to increase the coupling to the YIG resonators. Step transformers are used at the ends of the reduced-height section in order to provide a good impedance match. In some cases it may be necessary to space the spheres by approximately three quarter-wavelength instead of one quarter-wavelength, in order to avoid direct coupling between spheres.

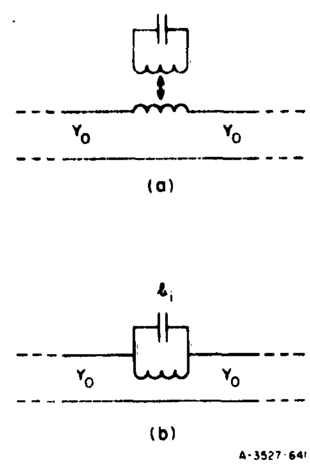

FIG. III-3 EQUIVALENT CIRCUITS OF A YIG SPHERE COUPLED TO A STRIP LINE AS SHOWN IN FIGS. III-2 AND III-4
In this figure, resonator losses are neglected

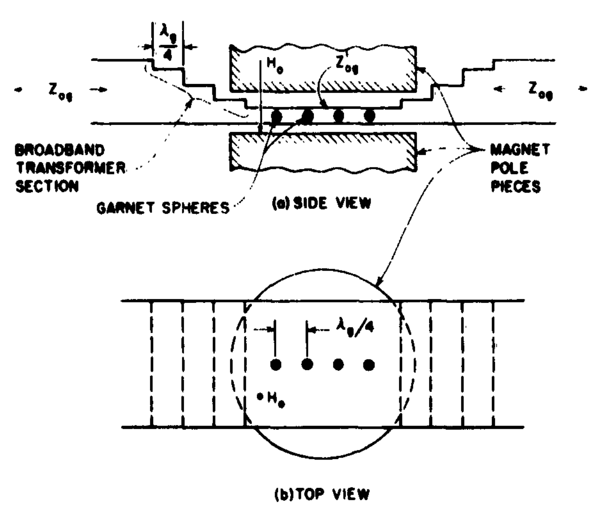

FIG. III-4 A FOUR-RESONATOR MAGNETICALLY TUNABLE WAVEGUIDE BAND-STOP FILTER

Figure III-5 shows another form of strip-line band-stop filter structure to be treated herein. In this case, part of the center conductor is replaced by a low-pass filter structure consisting of sections of high- and low-impedance transmission line, which simulate series inductances and shunt capacitances, respectively.[4,5] This configuration may make possible a more compact structure, so that smaller magnet pole faces can be used. It will be shown that this form of structure permits tighter coupling to the resonators (which will result in a broader stop-band width and higher mid-stop-band attenuation). A similar effect can be obtained in waveguide by using a corrugated waveguide filter structure.[6,5]

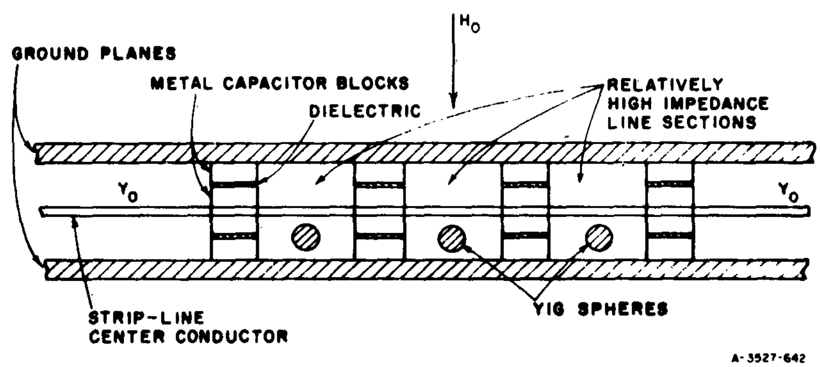

FIG. III-5 A SUGGESTED MAGNETICALLY TUNABLE BAND-STOP FILTER CONFIGURATION THAT PERMITS INCREASED COUPLING TO THE YIG SPHERES

B. BAND-STOP FILTER DESIGN EQUATIONS

We will now briefly define the necessary quantities and summarize the filter design equations needed for the design of magnetically tunable band-stop filters. Low-pass prototype filters, from which the band-stop filters discussed herein are designed, are shown at (a) and (b) in Fig. III-6. Note that the element values are defined in terms of parameters $g_0, g_1, g_2, \ldots, g_{n+1}$. Typical maximally flat and Chebyshev responses for such filters are shown at (c) and (d) in Fig. III-6. Note that a band-edge frequency ω_1' is specified. Element values for prototype low-pass filters of these types have been tabulated.[7,8]

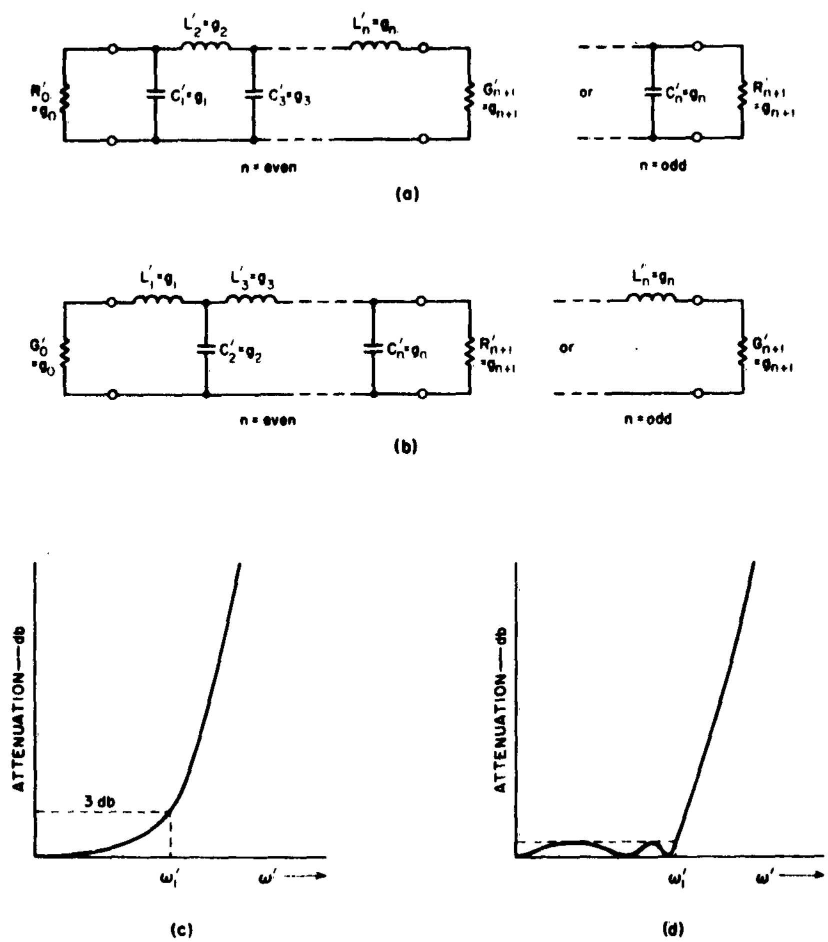

FIG. III-6 LOW-PASS PROTOTYPE FILTER
(a) and (b) Four basic circuit types, defining the parameters $g_0, g_1, \ldots, g_{n+1}$
(c) and (d) Maximally flat and equi-ripple characteristics, defining the band edge ω_1'

Figure III-7 shows the relations that will be used to obtain the band-stop filter design from the low-pass prototype. Note that the band-stop filter responses shown have a center frequency ω_0 corresponding to $\omega' = 0$ for the low-pass prototype, and band-edge frequencies ω_1 and ω_2, which correspond to the band-edge frequency ω_1' of the prototype. Equation (1), shown in Fig. III-7, can be used to map the response of the low-pass prototype into the corresponding response for the analogous band-stop filter.

A quarter-wave coupled band-stop filter using resonators of the form in Fig. III-3(b) is shown at (b) in Fig. III-7. The design equations necessary for the design of the filter from a low-pass prototype are also given. The resonators of the filter are characterized by their resonant frequency ω_0 (which is the same for all of the resonators) and and their *susceptance slope parameter* $\mathscr{b}_i$. The susceptance slope parameter of a resonator is defined as

$$\mathscr{b}_i = \frac{\omega_0}{2} \left.\frac{dB_i}{d\omega}\right|_{\omega=\omega_0} \qquad \text{(III-1)}$$

where B_i is the susceptance of the resonator. Note that $\mathscr{b}_i$ has the dimensions of susceptance; for a lumped-element resonator such as that in Fig. III-3(b), $\mathscr{b}_i = \omega_0 C_i$, where C_i is the capacitance of the capacitor. Equation (III-1), however, applies regardless of the form of the resonator, as long as the resonator exhibits a parallel-type of resonance (*i.e.*, $B_i = 0$ at resonance). If a resonator with a slope parameter of $\mathscr{b}_i$ is shunted by a conductance G_i, the Q of the combination is

$$Q_i = \frac{\mathscr{b}_i}{G_i} \quad . \qquad \text{(III-2)}$$

Equations (1) through (3) of Fig. III-7 can be used to map low-pass prototype filter responses[8] so as to find the number of resonators required to give the desired rate of cutoff, along with the desired form of pass-band characteristic. After a suitable low-pass prototype filter has been selected, the susceptance slope parameters required for the resonators of the band-stop filter can be computed in normalized form using Eqs. (4) and (5) of Fig. III-7. Note that for simplicity

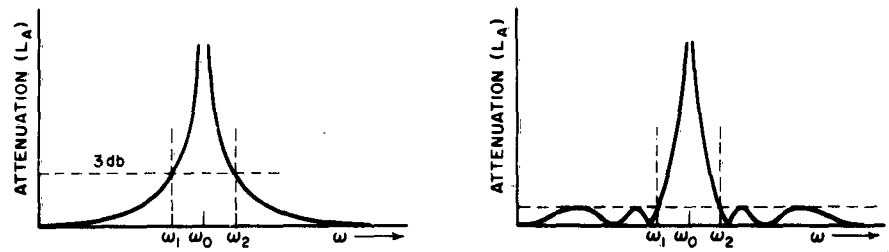

(a)

Mapping: $$\omega' = \frac{w\omega_1'}{2\left(\frac{\omega - \omega_0}{\omega_0}\right)} \quad (1)$$

where

$$\omega_0 = \frac{\omega_2 + \omega_1}{2} \quad (2)$$

$$w = \frac{\omega_2 - \omega_1}{\omega_0} \quad (3)$$

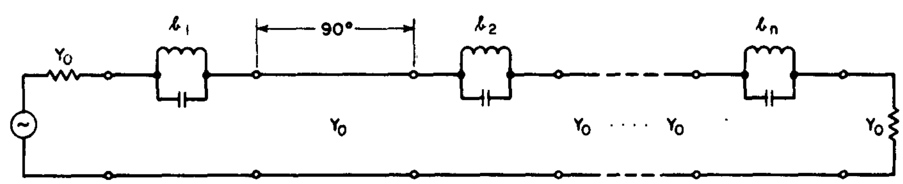

(b)

$$\left.\frac{b_i}{Y_0}\right|_{i=\mathrm{even}} = \frac{g_0}{\omega_1' g_i w} \quad (4)$$

$$\left.\frac{b_i}{Y_0}\right|_{i=\mathrm{odd}} = \frac{1}{\omega_1' g_0 g_i w} \quad (5)$$

where here $g_0 = g_{n+1}$ is required.

RA-4344-19

FIG. III-7 EQUATIONS FOR THE DESIGN OF BAND-STOP FILTERS FROM LOW-PASS PROTOTYPES and practicality, the equations in Fig. III-7 have been restricted to the case where $g_0 = g_{n+1}$. Chebyshev filters with n odd and all maximally flat filters satisfy this condition, provided that they are designed for minimum pass-band reflection loss. After the required normalized resonator slope parameters are determined, the required ferrimagnetic resonator properties can be determined, as explained in Part C of this discussion.

Because of the finite Q's of practical resonators, the attenuation at ω_0 does not go to infinity, but levels off at some finite value $(L_A)_{max}$ as indicated in Fig. III-1. To a good approximation,

$$(L_A)_{max} = 20 \log_{10} [(D_1 D_2 \ldots D_n)(g_1 g_2 \ldots g_n)] + 10 \log_{10} \left(\frac{4}{g_0 g_{n+1}}\right) \quad \text{db} \qquad \text{(III-3)}$$

where

$$D_i = w\omega_1'(Q_u)_i \qquad \text{(III-4)}$$

and $(Q_u)_i$ is the unloaded Q of the ith resonator.

A case of special interest is that where an equal-element prototype having $g_0 = g_1 = g_2 = \ldots g_{n+1} = 1$ is used. This leads to a band-stop filter having all of its resonators exactly the same. In this case, Eqs. (4) and (5) of Fig. III-7, and Eq. (III-3) above, reduce to

$$\left.\frac{\mathscr{b}_i}{Y_0}\right|_{i=1 \text{ to } n} = \frac{1}{\omega_1' w} \qquad \text{(III-5)}$$

and

$$(L_A)_{max} = 20n \log_{10} (w\omega_1' Q_u) \quad \text{db} \quad , \qquad \text{(III-6)}$$

respectively. If ω_1' is defined as the 3-db point of the low-pass prototype response, for equal-element prototypes with all $g_i = 1$, computations show that ω_1' varies with the number n of reactive elements as follows:

$$\begin{array}{llll} n = 1 & \omega_1' = 2 & n = 3 & \omega_1' = 1.52 \\ n = 2 & \omega_1' = 1.41 & n = 4 & \omega_1' = 1.65 \quad . \end{array} \qquad \text{(III-7)}$$

Using ω_1' defined in this way, w is the fractional bandwidth $w = \Delta f/f_0 = (\omega_2 - \omega_1)/\omega_0$, where Δf is the bandwidth at the 3-db points, as indicated in Fig. III-1. It is interesting to note from Eqs. (III-5) and (III-7) that, for a given resonator slope parameter for the resonator, adding one resonator so as to total two will *increase* the 3-db stop-band width by a factor of $\sqrt{2}$, but from there on, adding more resonators with the same slope parameter will cause the 3-db stop-band width to become narrower. However, adding more resonators will cause the peak attenuation $(L_A)_{max}$ to be larger, and the bandwidth at, say, the 20- or 30-db attenuation levels should be greater.

C. DETERMINATION OF FERRIMAGNETIC-RESONATOR AND COUPLING-STRUCTURE DIMENSIONS

If in Fig. III-3(b), a short circuit is placed across the transmission line just to the right of the resonator, and if the line to the left of the resonator is terminated in a conductance $G = Y_0$, by Eq. (III-2) the circuit will be seen to have a Q of

$$(Q_e)_i = \frac{\mathscr{b}_i}{Y_0} \quad . \tag{III-8}$$

The Q here has been designated Q_e because this Q corresponds to what is commonly called the *external* Q of a resonator, *i.e.*, the Q that a resonator would have if its internal losses were removed and it were loaded only by the external circuit to the left in Fig. III-3(b). Note that $(Q_e)_i$ above is the same as the normalized resonator slope parameters in Eqs. (4) and (5) of Fig. III-7, and in Eq. (III-5). Thus, we shall find that existing data for determining the external Q of YIG resonators in short-circuited strip-line and waveguide structures will prove very useful in band-stop filter design, as well as in the determination of the linewidth of ferrimagnetic crystals (a subject to be discussed in Part E). The short-circuit condition imposed to obtain Eq. (III-8) is, of course, hypothetical as far as band-stop filters are concerned. But imposing this hypothetical short-circuit provides a convenient way for establishing the $\mathscr{b}/Y_0$ ratio of a YIG resonator coupled to a line.

P. S. Carter Jr. has derived equations for the external Q of YIG ferrimagnetic resonators in strip-line and in waveguide structures[2] and has also prepared easy-to-use charts for certain cases.[9] Carter's charts[9] are reproduced in Figs. III-8 and III-9. The chart in Fig. III-8 gives the external Q of a YIG-sphere ferrimagnetic resonator in a 50-ohm strip-line structure, where the sphere is assumed to be placed close to a short-circuit in the structure, or at some multiple of a half-wavelength from the short-circuit. Figure III-8 gives Q_e for given sphere diameter D_m and strip-line to ground-plane spacing d, both in inches. The chart given applies specifically to a 50-ohm strip line and to YIG (which has a saturation magnetization of $4\pi M_s = 1750$ gauss). This chart can be adapted for use in other situations by use of the formula

$$Q_e = (Q_e)_{chart} \frac{50}{Z_0'} \left(\frac{Z_0}{Z_0'}\right) \left(\frac{1750}{4\pi M_s}\right) \tag{III-9}$$

where $(Q_e)_{chart}$ is the value of Q_e obtained from Fig. III-8 for the given values of d and D_m, Z_0' is the actual characteristic impedance of the strip line to which the ferrimagnetic sphere is coupled, and $4\pi M_s$ is the saturation magnetization of the ferrimagnetic material in gauss. The impedance Z_0 indicated in the formula will now be explained.

As mentioned in Part A, the filter in Fig. III-5 utilizes a low-pass filter structure having sections of high-impedance line to simulate series inductances, and sections of low-impedance lines to simulate shunt capacitances. Such structures can be designed on the image basis,[4] from lumped-element filter prototypes,[5,8] or from step-transformer prototypes.[5,10] In the pass band of this filter, the structure can be viewed as operating like an artificial transmission line of image impedance $Z_0 = 1/Y_0$, which corresponds to the characteristic impedance Z_0 of the uniform strip line in Fig. III-2. However, though the effective line impedance that the ferrimagnetic resonators observe is Z_0, the resonators are actually coupled to short line sections of much higher impedance Z_0'. Thus, if $Z_0 = 50$ ohms while $Z_0' = 100$ ohms, the resulting Q_e value will be $(50/100)^2 = 0.25$ times what it would be if the sphere were coupled to a uniform 50-ohm line (case of $Z_0 = 1/Y_0 = Z_0' = 50$). This Q_e value of one-fourth the size corresponds to a considerably tighter coupling between the line and the sphere, and would result in a broader stop-band width and higher peak attenuation $(L_A)_{max}$.

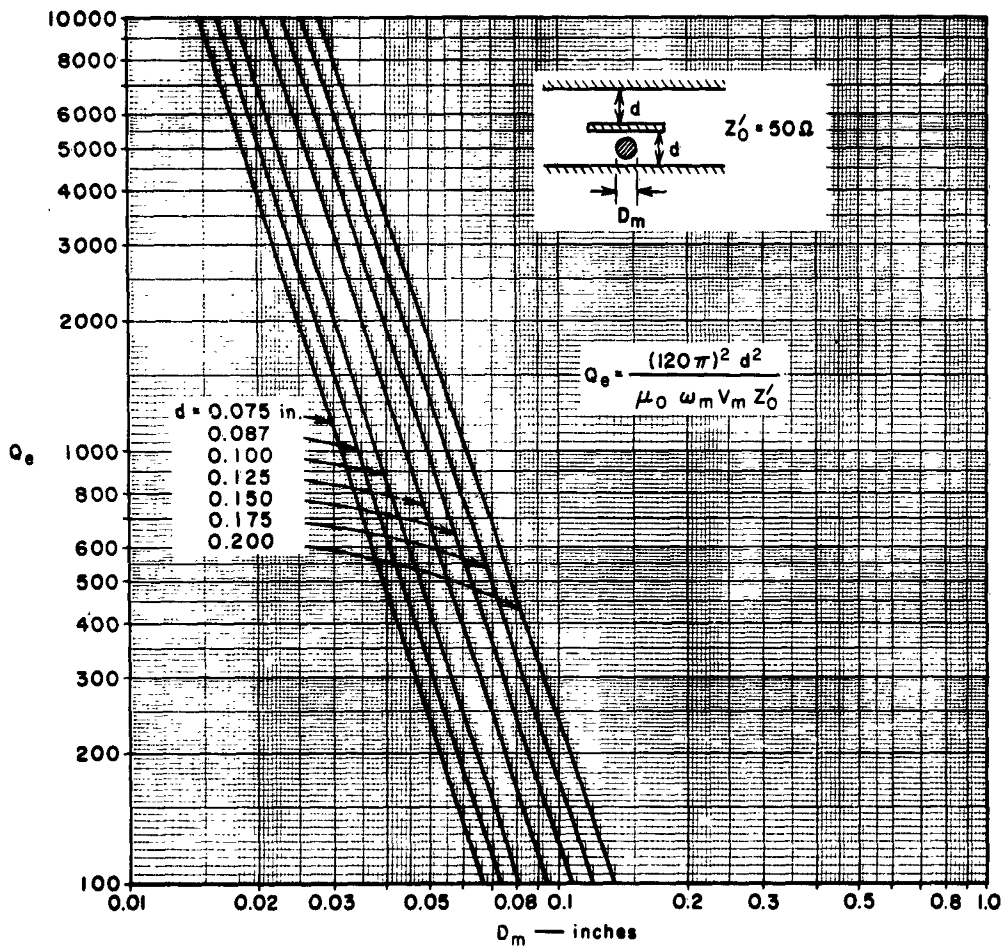

FIG. III-8 CARTER'S CHART OF Q_e vs. SPHERE DIAMETER FOR A SPHERICAL YIG RESONATOR IN SHORT-CIRCUITED, SYMMETRICAL STRIP TRANSMISSION LINE
In the equation shown, μ_0 is the permeability of the region about the sphere, $\omega_m = \gamma\mu_0 M_s$, $\gamma = 1.759 \times 10^{11}$ in mks units, V_m is the volume of the sphere, and Z_0, is the impedance of the strip line (Z_0, = 50 ohms for the graph)

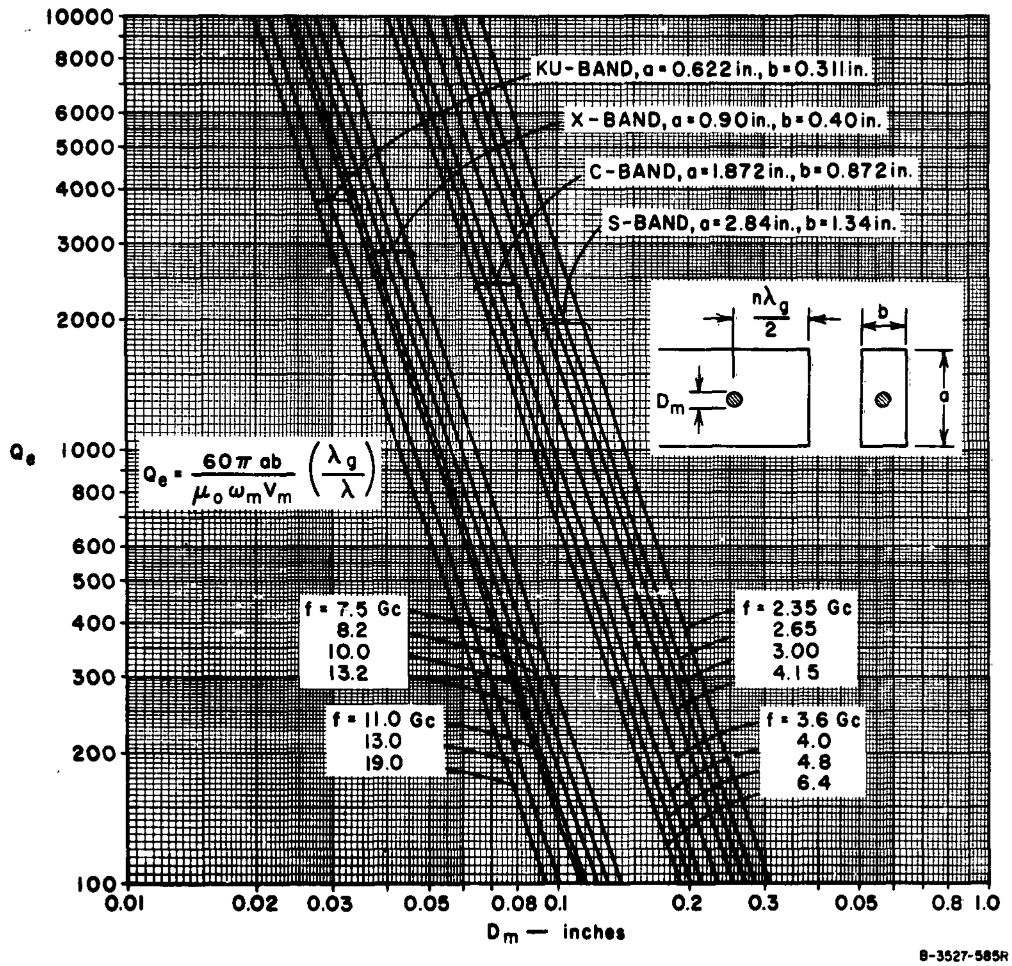

FIG. III-9 CARTER'S CHART OF Q_e vs. SPHERE DIAMETER OF SPHERICAL YIG RESONATOR LOCATED AT A HIGH-CURRENT POSITION IN SHORT-CIRCUITED TE_{10} RECTANGULAR WAVEGUIDE

In the equation shown, μ_0 is the permeability of the region about the sphere, $\omega_m = \gamma\mu_0 M_s$, $\gamma = 1.759 \times 10^{11}$ in mks units, and V_m is the volume of the sphere)

Carter's chart in Fig. III-8 was derived using a mathematical model, which assumed a strip line with no fringing capacitance. Thus, as the strip line becomes sufficiently narrow so that fringing effects influence the RF magnetic field seen by the sphere, the chart will become less accurate. Caution must also be taken in using too narrow a strip for coupling to the sphere because, if the RF magnetic field is very non-uniform, higher-order magnetostatic modes will be excited.

Figure III-9 shows an analogous chart for a YIG sphere next to a short circuit (or a multiple of a half wavelength from a short circuit) in *S*-band, *C*-band, *X*-band, and *KU*-band standard rectangular waveguide. In this case, Eq. (III-9) is replaced by

$$Q_e = (Q_e)_{\text{chart}} \left(\frac{b'}{b}\right) \left(\frac{b''}{b'}\right) \left(\frac{1750}{4\pi M_s}\right) \qquad \text{(III-10)}$$

where b is the height of standard guide as indicated in Fig. III-9, b' is the height of the guide actually used in the vicinity of the sphere, and b'' applies to the case where a corrugated waveguide structure is used[4,5,6] (which provides the analogous waveguide filter to the strip-line filter in Fig. III-5). The waveguide height b'' is the height of guide that would have the same characteristic impedance as the corrugated waveguide structure. If the waveguide structure is not corrugated, $b'' = b'$.

D. EXPERIMENTAL RESULTS

Two experimental strip-line structures were fabricated in order to test the theory discussed above. Filter 1 had the following construction and parameters:

(1) Physical form as in Fig. III-2, with a 50-ohm strip line having a strip-line to ground-plane spacing of $d = 0.110$ inch (and a ground-plane to ground-plane spacing of 0.240 inch).

(2) Two YIG-sphere resonators of diameter $D_m = 0.072$ inch located beneath the strip line and spaced 0.90 inch apart from center to center.

The YIG spheres were mounted on small dielectric rods, which could be rotated so as to tune both spheres to the same resonant frequency[11] (by adjusting the effect of the crystalline anisotropy field on the resonant frequency).

Table III-1

MEASURED PERFORMANCE OF BAND-STOP FILTER NO. 1
(The filter had two resonators and was of the form in Fig. III-2)

f_0 (Gc)	$(L_A)_{max}$ (db)	Δf MEASURED (Mc)	Δf COMPUTED (Mc)	APPROX. H_0 (oersted)*	MAJOR SPURIOUS RESPONSES
2.0	8.5	13.6†	8.3	730	2-db high at H = 700 oersted*
2.2	22.5	12.5	9.2	745	0.4-db high at H = 520 oersted*
3.0	32.0	15.2	12.5	1000	None observed
4.0	35.2	18.3	16.2	1450	0.1-db high at H = 1510 oersted*
5.0	36.8	19.4	20.3	1570	0.8-db high at H = 1720 oersted*
6.0	38.4	42.5†	24.3	1900	One, 1.4-db high for H = 2090 oersted. Another, 0.5-db high for H = 2200 oersted.*

* As measured approximately, with a gaussmeter.

† These oversized Δf values are believed to be due to the close proximity of spurious responses.

Table III-1 shows the measured results obtained with Filter 1. For resonance at f_0 = 2.0 Gc, the biasing magnetic field is not sufficiently large to permit very good operation, but above approximately f_0 = 2.2 Gc the performance is reasonably good. Note that $(L_A)_{max}$ is 32.0 db for f_0 = 3.0 Gc and increases for larger values of f_0. The 3-db bandwidth Δf (see Fig. III-1) was measured,* and also computed using Eqs. (III-5), (III-7) for n = 2, (III-8), and Fig. III-8 (which gave $Q_e \approx$ 170). Note that except for the sizeable errors at f_0 = 2.0 Gc and f_0 = 6.0 Gc, which are believed to be due to the proximity of spurious responses, the agreement between computed and measured values of Δf is reasonably good. Since spurious responses (see Fig. III-1) due to magnetostatic modes are always an important consideration in filters using ferrimagnetic resonators, the major spurious responses that were observed are noted on the right side of the table. These responses were observed by holding the signal frequency constant at the indicated value of f_0 while the

* In all the measured data in this part and in Part E, Δf was measured by interpolating from cavity wavemeter data using a swept signal generator and an oscilloscope. Thus the data for Δf are probably accurate to only plus or minus a few tenths of a megacycle.

biasing magnetic field was varied. Except at 2.0 Gc, which was out of the good operating range of the device (and possibly at 6.0 Gc, where there was a 1.4-db high response), the spurious response activity was quite small.

It is well known that if a ferrimagnetic resonator has sufficient power incident upon it, it ceases to perform as a high-Q resonator. (This property is utilized in YIG limiters.) In the case of a band-stop filter, this means that the attenuation of the resonators will disappear if the incident power is large enough. Figure III-10 shows the results of tests on Filter 1, which were made in order to determine the saturation characteristics of the filter. As expected, the attenuation dropped for a relatively small amount of incident power at 3000 Mc, but no saturation was observed at 6000 Mc for the amount of power available from the signal generator being used. The low saturation level, which occurs in the vicinity of S-band, is due to the fact that the spin-wave manifold

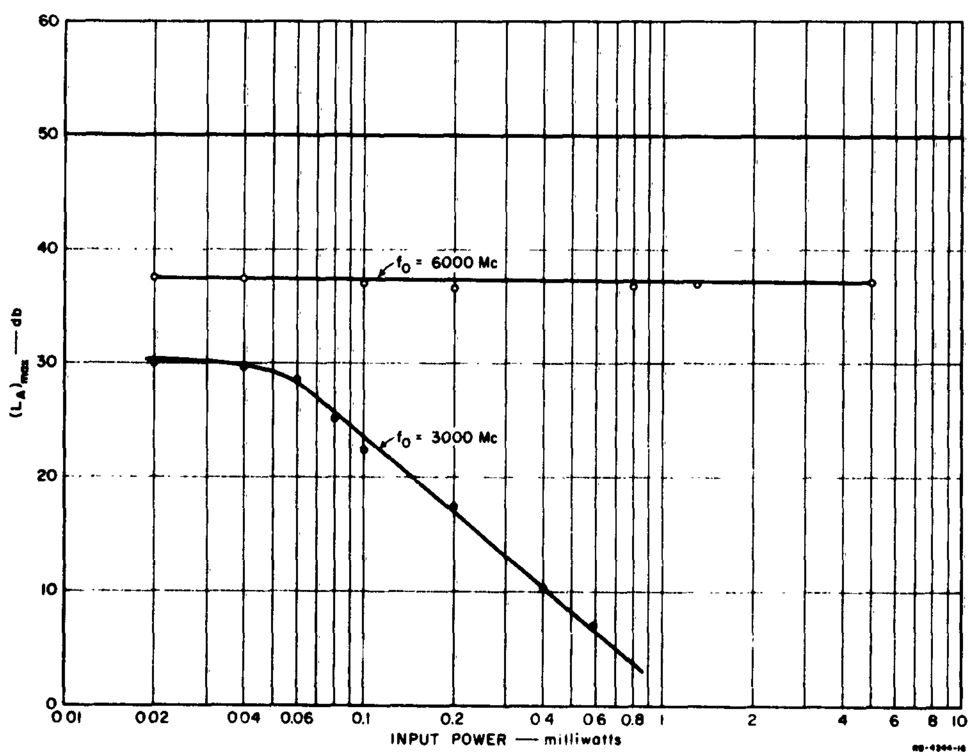

FIG. III-10 $(L_A)_{max}$ vs. INCIDENT POWER FOR FILTER 1 for YIG overlaps the uniform-precessional mode in this frequency range, and non-linear coupling sets in between the uniform-precessional mode and the spin-wave modes at quite low power levels.[12] Now the frequency range where there will be a large number of spin-wave modes with resonant frequencies which overlap that of the uniform precessional mode extends up to the frequency[12]

$$(f_0)_{Mc} = \left(\frac{2}{3}\right)(2.8)(4\pi M_s) \quad \text{Mc} \qquad \text{(III-11)}$$

(and somewhat beyond), where in this equation $4\pi M_s$ is in gauss. For YIG, which has $4\pi M_s = 1750$ gauss, Eq. (III-11) gives $(f_0)_{Mc} = 3270$ Mc. In order to prevent saturation effects from occurring at low power levels at S-band, it is necessary to use a ferrimagnetic material such as gallium-substituted yttrium-iron-garnet (Ga-YIG), which has a lower value of $4\pi M_s$. In the case of this particular device, no tests were made to determine the actual power levels for saturation at frequencies above S-band. However, Carter[13,2] found that in an X-band band-pass filter having a YIG resonator, 10 watts of incident power were required before saturation effects were apparent. In the case of an analogous X-band band-stop filter, saturation effects would be evident at a somewhat lower incident power level (estimates indicate at about a 6-db lower power level), but the saturation effects would probably increase with power very gradually if the band-stop filter had multiple resonators. This is because the second band-stop resonator would not saturate until the attenuation of the first band-stop resonator was very low, so as to let most of the incident power by. Also, the tighter the coupling between the transmission line and the ferrimagnetic resonators (*i.e.*, the smaller the b_i/Y_0), the larger will be the power handling ability of the filter. This is because as the resonator couplings get tighter, more power is reflected at resonance and less is absorbed by the resonators.

It was next desired to test the feasibility of increasing the coupling between a strip transmission line and a YIG sphere by coupling the sphere to a line of relatively high impedance Z_0' while the effective line impedance into which the sphere operates is a lower impedance Z_0. This is the situation discussed in Parts A and C above with respect to Fig. III-5. A rough approximation to this type of operation for the case of one YIG resonator was obtained by removing one of the YIG resonators of Filter 1

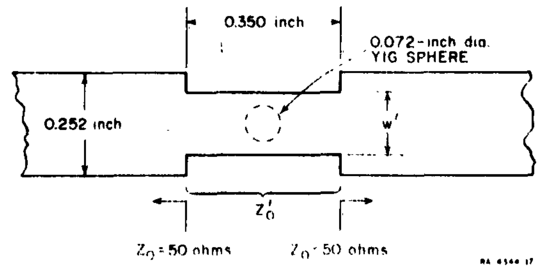

FIG. III-11 NOTCHING OF STRIP LINE TO INCREASE COUPLING TO A YIG RESONATOR

and notching the strip line in the vicinity of the other resonator, as shown in Fig. III-11. The sphere was coupled to a line section of impedance Z_0'; since the notched region was quite short, the terminating impedances seen by the sphere were still approximately 50 ohms (though, of course, as the notch was cut deeper greater deviation from this desired condition occurred). One of the main objectives of this experiment was to determine how narrow the strip line could be cut without causing a sizeable increase in spurious response activity. A secondary objective was to verify further the validity of the design theory discussed above.

As the depth of the notch in the strip line was increased, $(L_A)_{max}$ and the 3-db bandwidth Δf were measured for f_0 = 3000 and 4000 Mc, and checks were made to determine the location and size of any spurious responses. No appreciable increase in spurious response activity was noted until the strip was notched so that w' = 0.072 inch = diameter of sphere. For this case, the spurious responses rose from a few tenths of a db in height to somewhat over a db.

After approximating the resonator susceptance function by

$$B = 2b\left(\frac{f - f_0}{f_0}\right) \qquad \text{(III-12)}$$

where $\mathcal{b}$ is the resonator susceptance slope parameter, it is easily shown that for a single-resonator band-stop filter structure

$$\frac{\mathcal{b}}{Y_0} = Q_e \approx \frac{f_0}{2\Delta f} \qquad \text{(III-13)}$$

where Δf is the 3-db bandwidth defined in Fig. III-1. Table III-2 shows the values of $(L_A)_{max}$ and Δf measured for f_0 = 3000 Mc; the value of Q_e obtained from Eq. (III-13) above is compared with the value computed using Eq. (III-9). Note that by notching the strip line, very sizeable increases in $(L_A)_{max}$ and Δf were obtained, as expected; the values of Q_e computed from the measured data agree reasonably well with the data obtained using Fig. III-8 and Eq. (III-9).

Table III-2

EFFECT AT f_0 = 3000 Mc OF NOTCHING A 50-OHM STRIP LINE TO INCREASE COUPLING TO A YIG SPHERE

(A single 0.072-inch diameter YIG sphere was used and the line was notched as shown in Fig. III-11)

w' (inches)	Z'_0 (Ohms)	$(L_A)_{max}$ (db)	Δf (Mc)	$Q_e = \frac{f_0}{2\Delta f}$	Q_e BY EQ. (III-9)
0.252*	50*	12.5	9	167	170
0.152	74	20.8	17	88	78
0.102	93	24.5	28.6	52	49
0.072	110	24.0	36.8	41	35

* Case of no notch. In the design of the strip line, the fringing capacitance between the line and the side walls of the outer structure were taken into account, since the side walls were only 0.100 inch from the edges of the line when w' = 0.252 inch.

The experiment described above verified that the coupling to a ferrimagnetic resonator can be considerably increased in a strip-line structure if the sphere is coupled to a line section of relatively high impedance Z'_0, while the effective line impedance is of lower value Z_0. However, the notch shown in Fig. III-11 can cause an appreciable VSWR, and a low-pass structure, such as that in Fig. III-5, is preferable. To test this principle, Filter 2 (shown in Fig. III-12) was fabricated. This is a low-pass filter structure that was designed from a step-transformer prototype as discussed in Sec. 7.06 of Ref. 5, though other methods could also have been used. The structure of Filter 2 had the following properties:

(1) A Z_0 = 50-ohm input line was followed by a low-pass structure consisting of a short section of Z'_0 = 91 ohm line, followed by a low-impedance section of 26 ohms impedance, followed by another section of Z'_0 = 91 ohms, followed by an output line of Z_0 = 50 ohms. The low-pass structure was designed to match Z_0 = 50 ohms in its pass band.

(2) The cutoff frequency of the low-pass structure was 4000 Mc, so all desired signals should be below this frequency.

(3) The two 91-ohm line sections were each 0.221 inch long, and the 26-ohm line section used Rexolite 1422 dielectric and was 0.139 inch long. The 50-ohm input and output line sections used Rexolite 1422 dielectric for rigidity.

(4) Provision was made for mounting a YIG sphere on a rod at the center of each Z'_0 = 91-ohm line section. In order to reduce possible coupling between the two spheres, one sphere was mounted above, the other below its adjacent 91-ohm line section. The resonators were each mounted with a [110] crystal axis parallel to the mounting rod axis; the resonators were tuned by rotating the spheres about this axis (which was perpendicular to the biasing field H_0).[11]

When the filter was tested with two spheres, it was found that there was appreciable direct coupling between the spheres, in spite of efforts to avoid this difficulty. This coupling evidenced itself by interaction between the two spheres when either was tuned. Because of this, only one resonator could be used satisfactorily in this structure.

Tests were made on Filter 2 using one YIG sphere; Table III-3 summarizes the results. Note that the measured and computed values of Q_e again agree reasonably well. The quantity on the right is the unloaded Q, Q_u. This was computed from the measured data by procedures (to be discussed in Part E, following).

In order for a filter structure such as Filter 2 to work satisfactorily with two or more spheres, it appears that the spheres would have to be spaced so that the electrical distance between them is approximately $3\pi/2$ radians instead of $\pi/2$ radians in the operating range. This would

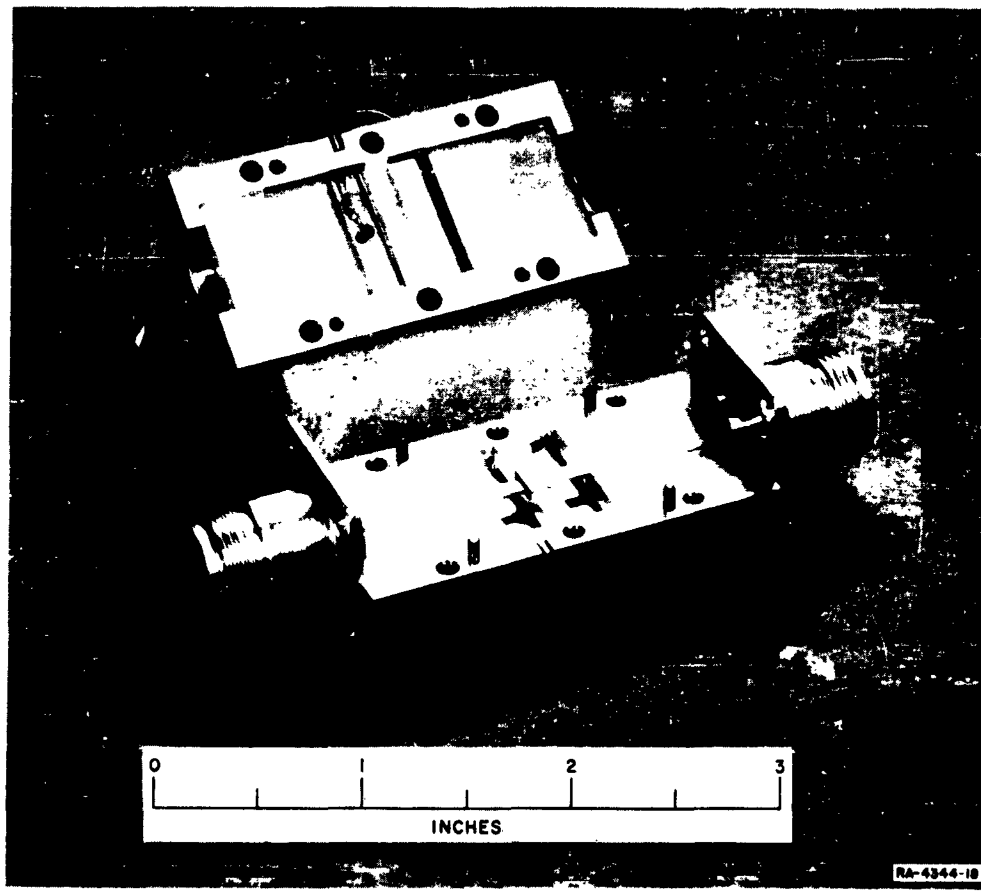

FIG. III-12 FILTER 2, WHICH UTILIZES A LOW-PASS FILTER STRUCTURE TO ENHANCE THE COUPLING BETWEEN THE MAIN LINE AND EACH YIG SPHERE
A YIG sphere is shown mounted in the structure

Table III-3

MEASURED RESULTS OBTAINED ON THE FILTER STRUCTURE IN FIG. III-12 USING ONE 0.072-INCH DIAMETER YIG RESONATOR

f_0 (Mc)	Δf (Mc)	$(L_A)_{max}$ (db)	$Q_e = \dfrac{f_0}{2\Delta f}$	Q_e BY EQ. (III-9)	Q_u
2200	26.2	11.8	42.0	49.0	283
3000	26.7	21.3	56.2	49.0	1039
4000	41.3	23.5	48.5	49.0	1460

make the direct coupling between resonators negligible, but this arrangement would also tend to limit further the tuning range over which full use of the resonators can be made. (If two band-stop resonators are separated by an odd multiple of $\pi/2$ resonators, the total db peak attenuation will be approximately twice the db peak attenuation of either resonator alone. If two resonators are separated by a multiple of π radians, the total db peak attenuation will be only about 5 db more than that for one resonator alone.) However, if the structure had been fabricated more as shown in Fig. III-5, where metal capacitor blocks are used, the metal blocks might have been helpful in eliminating direct coupling between resonators. (In Fig. III-5, mounting the middle sphere above the strip line instead of below should also help.)

E. A SIMPLE PROCEDURE FOR MEASURING THE LINEWIDTH OF GARNET RESONATORS

Operating a garnet sphere as a single-resonator band-stop filter provides a simple means for determining the resonance linewidth ΔH of the garnet material. We shall now describe the necessary equations and procedures.

The effect of the internal loss in a garnet resonator in a band-stop filter can be represented by a conductance G_s in parallel with the L and C in Fig. III-3(b). Then the unloaded Q of such a resonator is $Q_u = b/G_s$, where b is the resonator susceptance slope parameter. Using this definition of Q_u, along with $Q_e = b/Y_0$, by straightforward circuit analysis it is easily shown that, for a single-resonator band-stop filter,

$$Q_u = 2Q_e(A - 1) \qquad \text{(III-14)}$$

where

$$A = \text{antilog}_{10} \frac{(L_A)_{max}}{20} \qquad \text{(III-15)}$$

and $(L_A)_{max}$ was defined in Fig. III-1. Now Q_u can also be expressed as

$$Q_u = \frac{H_0}{\Delta H} \qquad \text{(III-16)}$$

where H_0 is the dc biasing field strength at resonance, and ΔH is the resonance linewidth.[1] Neglecting the effect of the anisotropy field on the frequency of resonance,

$$H_0 = \frac{(f_0)_{Mc}}{2.8} \quad \text{oersted} \qquad \text{(III-17)}$$

where $(f_0)_{Mc}$ is in megacycles. By Eqs. (III-14), (III-16), and (III-17),

$$\Delta H = \frac{(f_0)_{Mc}}{5.6 Q_e (A - 1)} \quad \text{oersted} \quad . \qquad \text{(III-18)}$$

Since for strip-line and waveguide configurations, Q_e can be obtained directly from the information in Part C of this discussion, ΔH can be determined by measuring $(L_A)_{max}$ and then computing ΔH from Eq. (III-18).

This writer (G. L. Matthaei) found from discussions with Dr. K. L. Kotzebue of the Watkins-Johnson Co. that Dr. Kotzebue has been obtaining linewidth measurements by making band-stop tests, then applying the approximate formula

$$\Delta H = \frac{(\Delta f)_{Mc}}{2.8 A} \quad \text{oersted} \qquad \text{(III-19)}$$

where $(\Delta f)_{Mc}$ is the bandwidth defined in Fig. III-1 in megacycles, and A is given by Eq. (III-15). Equation (III-19) can be derived from Eqs. (III-16), (III-17) and Eq. (8) of Ref. 14 (by Kotzebue). Because of certain approximations involved, this formula should be most accurate if $(L_A)_{max}$ is sizeable.

Dr. Kotzebue and this writer made some trial tests and compared the two procedures just discussed. The results were in encouragingly good agreement. For example, Table III-4 shows the results of a series of tests on garnet spheres tested in standard X-band waveguide. The spheres were mounted in the guide by inserting them in a piece of polyfoam, which was slipped into the guide. No effort was made to orient the crystal axes in any special way. For each case, $(L_A)_{max}$ and Δf were measured, and ΔH was computed both by Eq. (III-18) and (III-19). Note that the two values of ΔH are, for the most part, in good agreement, especially when considering that the accuracy in measuring Δf was probably only to a few tenths of a megacycle.

Table III-4

RESULTS OF SOME LINEWIDTH TESTS ON YIG AND Ga-YIG SPHERES IN X-BAND WAVEGUIDE

MATERIAL	SPHERE DIAMETER (inches)	$(L_A)_{max}$ (db)	Δf (Mc)	ΔH, EQ. (III-18) (oersted)	ΔH, EQ. (III-19) (oersted)
YIG	0.072	19.5	11.0	0.43	0.42
Ga-YIG $4\pi M_s$ = 920 Gauss	0.071	10.5	6.7	0.71	0.71
YIG	0.049	11.6	3.5	0.35	0.33
YIG	0.049	11.6	3.0	0.35	0.28
YIG	0.041	7.7	3.5	0.44	0.52

Due to certain approximations involved, Eq. (III-19) can be expected to deteriorate in accuracy if $(L_A)_{max}$ is not sufficiently large [*i.e.*, probably $(L_A)_{max}$ should be around 10 db or more]. Some experimental results suggest that Eq. (III-18) will also give better results if $(L_A)_{max}$ is around 10 db or preferably larger (though the need for this has not been fully checked at this time). Thus, it is recommended that a waveguide or strip-line structure be used that will give a reasonably tight coupling between the sphere and the structure. (A Q_e value between 500 and 1000 is satisfactory at X-band for most cases.) In waveguide structures, reduced height waveguide will be required in cases where the waveguide cross-sectional dimensions are very large compared to the sphere diameter, but caution should be taken that the height of the guide is not reduced so much that the close proximity of the metal walls degrades the unloaded Q of the garnet resonator. A guide height of three times the diameter of the sphere is probably safe. Similar considerations hold when making tests using strip-line structures. Caution should also be taken to ensure that tests are not made at frequencies where a spurious response is very close to the main response.

The two test procedures described above are both quite simple and easy to use, but the one based on Eq. (III-18) appears to be especially convenient, since it only requires that $(L_A)_{max}$ be measured (no bandwidth measurements are needed). As can be seen from Table III-3, the tests can be made in standard X-band waveguide for the more common sizes of YIG spheres, and no special test devices are required

Mr. Ernest Stern of the Microwave Chemicals Laboratory, Inc. has informed this writer (G. L. Matthaei) that H. E. Bussey of the U.S. Bureau of Standards, Boulder, Colorado has also developed a procedure for testing YIG spheres, which requires only an attenuation measurement. Mr. Stern also reports that Bussey's procedure is frequently used by YIG material manufacturers. Though Bussey's procedure and that described here involve the same fundamental physical principles, his procedure apparently uses a different analytical point of view and has been based on the use of a special test cavity. The procedure outlined herein appears to have advantages in that for many cases no special test device will be required and the calculations involved are reduced to a minimum.

REFERENCES

1. B. Lax and K. J. Button, *Microwave Ferrites and Ferrimagnetics*, McGraw-Hill Book Co., Inc., New York (1962).

2. P. S. Carter, Jr., "Magnetically Tunable Microwave Filters Using Single-Crystal Yttrium-Iron Garnet Resonators," *IRE Trans. PGMTT*-**9**, pp. 252-260 (May 1961).

3. Leo Young, G. L. Matthaei, and E. M. T. Jones, "Microwave Bandstop Filters with Narrow Stop Bands," *IRE Trans. PGMTT*-**10**, pp. 416-427 (November 1962).

4. Harvard Univ. Radio Research Laboratory Staff, *Very High-Frequency Techniques*, Vol. 2 (McGraw-Hill Book Co., Inc., New York, 1947), pp. 769-795.

5. G. L. Matthaei, L. Young, and E. M. T. Jones, *Design of Microwave Filters, Impedance-Matching Networks, and Coupling Structures*, a book prepared on SRI Project 3527, Contract DA 36-039 SC-87398, Stanford Research Institute, Menlo Park, California (January 1963), Chapter 7.

6. S. B. Cohn, "Design Relations for the Wide-Band Waveguide Filter," *Proc. IRE* **38**, pp. 799-803 (July 1950).

7. L. Weinberg, "Additional Tables for Design of Optimum Ladder Networks," Parts I and II, *J. Franklin Institute* **264**, pp. 7-23 and 127-138 (July and August 1957).

8. G. L. Matthaei, Leo Young, E. M. T. Jones, *loc. cit.*, Chapter 4.

9. B. M. Schiffman, P. S. Carter, Jr., and G. L. Matthaei, "Microwave Filters and Coupling Structures," Seventh Quarterly Progress Report, Part III, SRI Project 3527, Contract DA 36-039 SC-87398, Stanford Research Institute, Menlo Park, California (October 1962).

10. G. L. Matthaei, Leo Young, and E. M. T. Jones, *loc. cit.*, Chapter 6.

11. *Ibid.*, Chapter 17.

12. H. Suhl, "The Nonlinear Behavior of Ferrites at High Microwave Signal Levels," *Proc. IRE* **44**, pp. 1270-1284 (October 1946).

13. G. L. Matthaei, ..., P. S. Carter, Jr., *et al.*, "Design Criteria for Microwave Filters and Coupling Structures," Chap. 28, Final Report, SRI Project 2326, Contract DA 36-039 SC-74862, Stanford Research Institute, Menlo Park, California (January 1961).

14. K. L. Kotzebue, "Broadband Electronically-Tunable Microwave Filters," *1960 IRE WESCON Convention Record*, Part 1, pp. 21-27.

IV VOLTAGE-TUNABLE FILTERS AND PHASE SHIFTERS

A. GENERAL

Voltage-variable capacitors (varactor diodes) have been employed for a number of years as electronic tuning elements. Unfortunately, the so-called spreading resistance of the diode, which is effectively in series with the diode capacitance, causes the circuit performance of any given varactor to become poorer as operating frequency is increased. Also, each diode is limited in its range of capacitance variations. These two characteristics combine to limit the use of varactor-tuned circuits at microwave frequencies. One can expect, however, that solid state technology will greatly improve the quality of these circuit elements so that, in time, their use will be greatly expanded.

Although highly selective voltage-tunable band-pass filters having low insertion-loss cannot yet be constructed with varactor diodes at microwave frequencies,[1,2*] a varactor-tuned resonant circuit, which is either too lossy for a narrow-band filter or incapable of sufficient tuning range in a moderately wide-band filter, is still useful as a phase shifter. This is explained by the fact that while there will be negligible change in attenuation, there can be a large change in phase shift if the pass band is tuned to move back and forth a small amount. A relatively small tuning range is required to obtain a useful amount of phase shift, because the total phase variation with frequency is 180 degrees per resonator with most of the variation occurring in and near the pass band. Thus, a band-pass filter consisting of several resonant circuits should be tunable so that a phase change of (plus or minus) 90 degrees or more is obtained (at a given center frequency) with negligible change in signal level. It would be necessary to tune the center frequency by some amount less than the filter bandwidth and still maintain the shape of the pass band sufficiently well so that dissipation loss at center frequency remains unchanged.

In view of the above prospects and possibilities, Part B and C discuss circuit configurations that could be used for either band-pass filters or phase-shifters. Tuning range and dissipation loss are considered. Part D gives some numerical examples.

---

* References for Sec. IV are grouped at the end of the section.

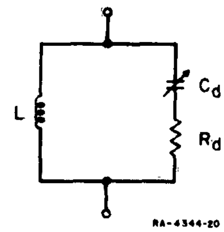

FIG. IV-1 A RESONATOR WITH DIODE-CAPACITANCE TUNING – THE Q OF THE RESONATOR EQUALS THE Q OF THE DIODE

B. RESONANT CIRCUITS EMPLOYING VOLTAGE-VARIABLE DIODES

Figure IV-1 shows a parallel LC resonant circuit in which the varactor diode comprises the total circuit capacitance. Q_u, the Q of the unloaded circuit, equals Q_d, the Q of the diode; the circuit losses occur mainly in the diode series resistance R_d. As the circuit is tuned, it is seen from the equation

$$Q_u = \omega_r L/R_d \qquad \text{(IV-1)}$$

that Q_u increases with frequency of resonance ω_r. Here both L and R_d are fixed. The tuning ratio, maximum frequency to minimum frequency, is

$$\rho = (C_2/C_1)^{1/2} \qquad \text{(IV-2)}$$

It can be easily shown that Q_u can be substantially increased above Q_d, provided the tuning ratio ρ is reduced. Two lumped-element circuits that accomplish this increase are shown in Figs. IV-2 and IV-3. Design curves relating bandwidth and Q-multiplication factor for these circuits are given in Ref. 2. In the circuit of Fig. IV-2, the diode capacitance C_d is greater than the total circuit capacitance consisting of C_d and C_s in series, while in the circuit of Fig. IV-3, the diode capacitance is less than the total circuit capacitance. Thus, by means of one of the circuits in Figs. IV-1 to IV-3, any of a wide variety of diodes can be used to tune a resonant circuit in a given frequency band. Of course, the tuning ratio and Q_u are different in each case and the optimum choice depends both on those values and circuit complexity. However, no matter what choice is made, one finds that Q_u increases more or less rapidly with frequency when the circuit is tuned by changing C_d.

A circuit that employs a transmission line[2] in place of the added inductor and capacitor of the previously mentioned circuits is shown in Fig. IV-4. In this circuit, as in the lumped-element circuit, Q_u is enhanced. Not only is the Q_u of this circuit greater than the diode Q, but the designer has sufficient circuit parameters available that he can favor either the low end or the high end of the tuning range with respect to enhancing the diode Q. This is accomplished by judicious choice of Z_0, θ' and n in Fig. IV-4. It is, of course, necessary to satisfy the resonance equation

$$\tan \theta' = 1/\omega C_d Z_0 \qquad \text{(IV-3)}$$

where the electrical length $\theta' < \pi/2$. (Although the total length of transmission line is constant, the nodal point shifts as frequency is changed and the quantity θ' is thus a somewhat complex function of frequency.)

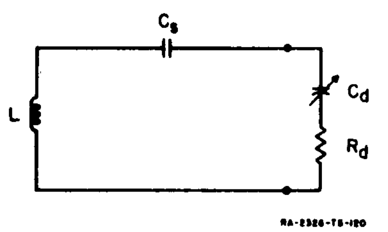

FIG. IV-2 A RESONATOR WITH DIODE-CAPACITANCE TUNING AND AN EXTRA CAPACITANCE C_S TO ENHANCE THE Q OF THE DIODE

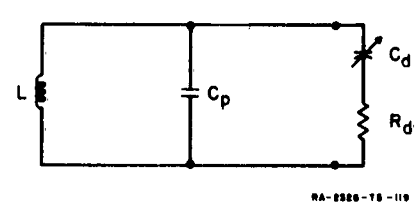

FIG. IV-3 A RESONATOR WITH DIODE-CAPACITANCE TUNING AND AN EXTRA CAPACITANCE C_P TO ENHANCE THE Q OF THE DIODE

C. TWO NEW CIRCUITS THAT ALLOW ADDITIONAL DESIGN FLEXIBILITY

The variation of the resonator Q_u with frequency is determined by the particular circuit and element values chosen; although many choices are available to the designer in circuits of Figs. IV-1, IV-2, and IV-3, the Q_u at each end of the tuning range is always different sometimes greatly so. However, greater design flexibility is afforded by the circuit of Fig. IV-4 with respect to controlling this Q-variation. This design flexibility can also be obtained in a slightly more complex

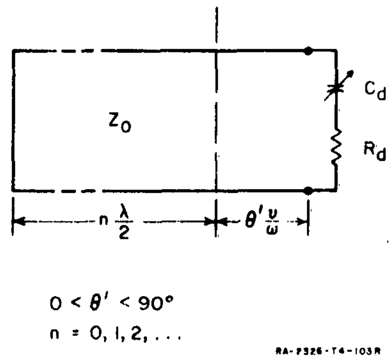

FIG. IV-4 A TRANSMISSION LINE RESONATOR TUNED BY THE BARRIER CAPACITANCE OF A BACK-BIASED DIODE

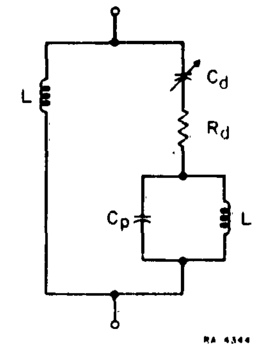

FIG. IV-5 A RESONATOR WITH A PARALLEL (L_pC_p) NETWORK IN SERIES WITH THE VARACTOR TO ENHANCE THE DIODE Q IN A CONTROLLED MANNER

lumped-element resonator circuit, as shown in Fig. IV-5. The circuit of Fig. IV-4 also can be slightly modified to produce the circuit of Fig. IV-6. These circuits can be designed to increase Q_u above Q_d with a Q-multiplication factor that can be independently controlled for two points in the tuning range, as explained below.

In Fig. IV-5, an auxiliary circuit composed of inductor L_p and capacitor C_p in parallel is in series with the main inductor L and the varactor diode. The resonant frequency $\omega_p = 1/\sqrt{L_pC_p}$ of the auxiliary circuit L_pC_p is below the parallel-resonant frequency ω_r for the over-all circuit, and has an effect on ω_r similar to the series capacitor C_s of the circuit of Fig. IV-2. However, the auxiliary circuit susceptance is not a linear function of frequency, as is the susceptance of a capacitor. In the limit (the case of a very low resonant frequency of the auxiliary circuit) its effect in the network at the operating frequency approaches that of a series capacitance, while for a resonant frequency that is close to but slightly less than the operating frequency, its effect is more complex. In particular, it tends to raise the circuit Q

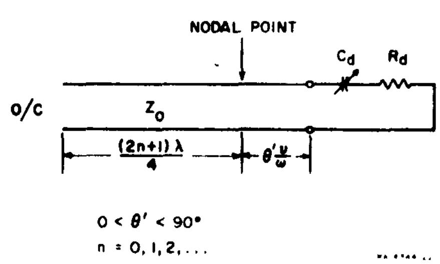

FIG. IV-6 AN OPEN-CIRCUITED TRANSMISSION LINE RESONATOR TUNED BY DIODE CAPACITANCE more near the low end of the tuning range than near the high end. The expression for Q_u of the circuit in Fig. IV-5 is, for any frequency of resonance ω_r,

$$Q_u = \frac{\alpha}{R_d} \tag{IV-4}$$

where the reactance slope parameter[3] α is defined (in the notation used here)

$$\alpha = \frac{\omega_r}{2} \frac{dX}{d\omega}\bigg|_{\omega=\omega_r} \tag{IV-5}$$

and X, the total series reactance, is given by

$$X = \omega L - \frac{1}{\omega C_d} + \left(\frac{L_p}{C_p}\right)\frac{1}{\omega L_p - 1/\omega C_p} \quad . \tag{IV-6}$$

The factor on the right in Eq. (IV-5) is found to be

$$\frac{dX}{d\omega}\bigg|_{\omega=\omega_r} = 2\left[L + \frac{1}{L_p}\left(\frac{\omega_r^2 C_d L - 1}{\omega_r^2 C_d}\right)^2\right] \quad , \tag{IV-7}$$

from which equation, combined with Eqs. (IV-4) and (IV-5), the Q_u of the circuit may be obtained. The behavior of $dX/d\omega$ can be easily visualized by examining Fig IV-7, which is a plot of the reactance X for the two cases where ω_p is near and far from the operating range. It is evident that the slope of the curves of the circuit reactance at a resonant frequency (the figures show X for the two cases where the varactor is tuned for circuit resonance at ω_1 and ω_2) is little affected by the pole at ω_p in Fig. IV-7(b). In Fig. IV-7(a), where ω_p is close to the operating range, the slope at resonance is much affected by the nearby pole ω_p, particularly at the lower portion of the operating range, as indicated by the dashed curve with resonant frequency ω_1 in Fig. IV-7(a). Note the spurious pass band below ω_p in Fig. IV-7.

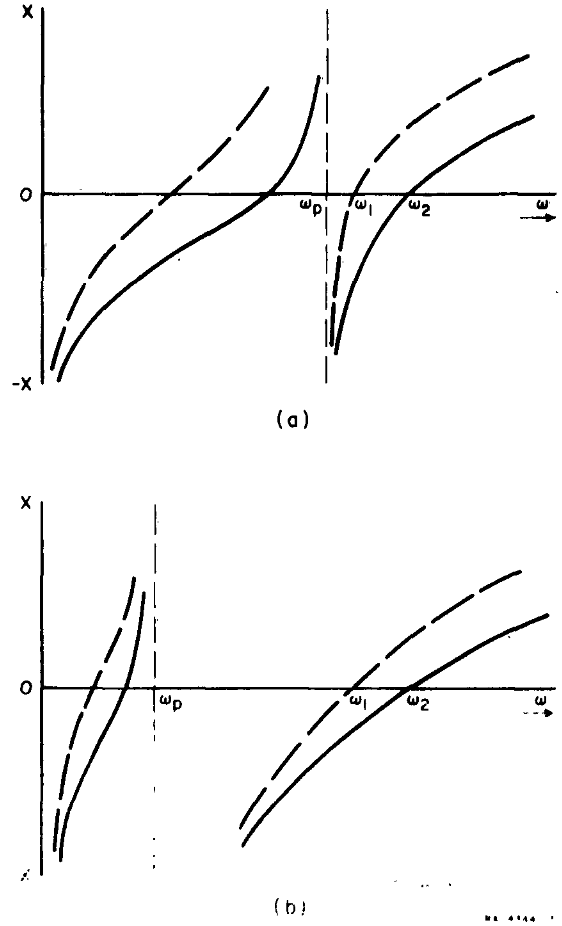

FIG. IV-7 LOOP REACTANCE DIAGRAMS OF CIRCUIT OF FIG. IV-5

The transmission-line resonator circuit of Fig. IV-6 is similar to that of Fig. IV-4, except that the short-circuit termination of Fig. IV-4 is replaced by an open-circuit in Fig. IV-6. All other things being equal, the total line lengths for the two circuits must differ by $\lambda_0/4$ and the corresponding Q_u must be different (in the same sense). It is reasonable to suppose, therefore, that the design graphs that give the Q-multiplication factors for the circuit of Fig. IV-4[2] can be adapted for the circuit of Fig. IV-6 by interpolation. For example, a curve for the circuit in Fig. IV-6 could be sketched in about midway between curves $n = 1$ and $n = 2$ in Fig. 27-7, p. 458, of Ref. 2. The approximate bandwidth contraction factor for this circuit could be obtained by interpolating between Figs. 27-4, -5, and -6 in Ref. 2.

D. A DESIGN EXAMPLE

In order to compare the circuit of Fig. IV-5 with the earlier forms of resonators shown in Figs. IV-2 and IV-3, a design example was worked out using the same input data that was used in designing the latter two circuits (see Table IV-1). For the particular diode chosen,

Table IV-1

COMPARISON OF RESONATOR Q's OBTAINED WITH THE CIRCUITS OF FIGS. IV-2, IV-3, AND IV-5

Example: $(C_{d_{max}}/C_{d_{min}}) = 2.5$, $(Q_d)_{min} = 40$, $(Q_d)_{max} = 100$

For Frequency Range 1000 to 1100 Mc

TYPE OF RESONATOR	$(Q_u)_{\omega=\omega_{min}}$	$(Q_u)_{\omega=\omega_{max}}$
Fig. IV-2	138	710
Fig. IV-3	284	347
Fig. IV-5	300	300

with $C_{d_{min}} = C_{d1} = 10$ pf and $C_{d_{max}} = C_{d2} = 25$ pf, the values of Q_u at the extremes of the tuning range were made to be equal with $Q_u = 300$ for the circuit of Fig. IV-5. This compares with the unequal values of Q_u at the extremes of the tuning range for the other two circuits. The element values for the circuit of Fig. IV-5 are $L = 0.00585$ μh, $L_p = 0.0134$ μh, $C_p = 7.4$ pf. The parallel resonant frequency of the auxiliary circuit is $f_p = 510$ Mc.

These design values were obtained by the following method: We first note that there are three conditions to be fulfilled, namely, the circuit must be resonant at 1000 Mc when $C_{d2} = 25$ pf, and at 1100 Mc when $C_{d1} = 10$ pf, and the Q_u's must be equal at these frequencies. The resonance condition is given mathematically by setting Eq. (IV-7) equal to zero at ω_1 and ω_2.

Thus

$$\omega_1 L - \frac{1}{\omega_1 C_{d2}} + \left(\frac{L_p}{C_p}\right) \frac{1}{\omega_1 L_p - 1/\omega_1 C_p} = 0 \qquad \text{(IV-8)}$$

and

$$\omega_2 L - \frac{1}{\omega_2 C_{d1}} + \left(\frac{L_p}{C_p}\right) \frac{1}{\omega_2 L_p - 1/\omega_2 C_p} = 0 \quad . \qquad \text{(IV-9)}$$

The equal Q_u condition is obtained from Eqs. (IV-4), (IV-5) and (IV-7):

$$\omega_1 \left[L + \frac{1}{L_p}\left(L - \frac{1}{\omega_1^2 C_{d2}}\right)^2\right] = \omega_2 \left[L + \frac{1}{L_p}\left(L - \frac{1}{\omega_2^2 C_{d1}}\right)^2\right] \quad . \qquad \text{(IV-10)}$$

Although an explicit solution is possible, the quadratic form of Eq. (IV-10) makes the mathematics involved; therefore, a graphical solution was obtained with the aid of the following three equations [derived from Eqs. (IV-8) through (IV-10)]:

$$L = \frac{1}{\omega_2^2 - \omega_1^2} \left\{\left[1 - \left(\frac{\omega_p}{\omega_2}\right)^2\right] \frac{1}{C_{d1}} - \left[1 - \left(\frac{\omega_p}{\omega_1}\right)^2\right] \frac{1}{C_{d2}}\right\} \quad , \qquad \text{(IV-11)}$$

$$L_p = L\left\{\frac{\omega_1}{\omega_2 - \omega_1}\left(1 - \frac{1}{\omega_1^2 L C_{d2}}\right)^2 - \frac{\omega_2}{\omega_2 - \omega_1}\left(1 - \frac{1}{\omega_2^2 L C_{d1}}\right)\right\}^2 \qquad \text{(IV-12)}$$

and

$$L_p = \left[L - \frac{1}{\omega_1^2 C_{d2}}\right] \left[\left(\frac{\omega_1}{\omega_p}\right)^2 - 1\right] \quad . \qquad \text{(IV-13)}$$

Finally, C_p is calculated from

$$C_p = \frac{1}{\omega_p^2 L_p} \quad . \tag{IV-14}$$

Equation (IV-11) was obtained from Eqs. (IV-8) and (IV-9) (after first making the substitution $\omega_p^2 = 1/L_p C_p$), by solving each for L_p, equating the resulting expressions and then solving for L. Equation (IV-12) is Eq. (IV-10) rearranged, and Eq. (IV-13) is Eq. (IV-8) rearranged, with the above substitution made here also. When a pair of values of ω_p and L that satisfy Eq. (IV-11) are found to yield the same value of L_p in Eqs. (IV-12) and (IV-13), the problem is solved. As a check, the values of Q_u are calculated at ω_1 and ω_2.

REFERENCES

1. S. B. Cohn, "Electronic Tuning of Filters—Basic Limitations," *Microwave Journal*, **5**, p. 17 (November 1962).

2. G. L. Matthaei, *et al.*, "Design Criteria for Microwave Filters and Coupling Structures," Final Report, SRI Project 2326, Contract DA 36-039 SC-74862, Stanford Research Institute, Menlo Park, California (June 1957).

3. G. L. Matthaei, L. Young, and E. M. T. Jones, *Design of Microwave Filters, Impedance Matching Networks, and Coupling Structures*, a book prepared on SRI Project 3527, Contract DA 36-039 SC-87398, Stanford Research Institute, Menlo Park, California (January 1963), Vol. I, Sec. 8.02.

V MEASURED PERFORMANCE OF A CAPACITIVELY LOADED INTERDIGITAL FILTER

A. FILTER DESIGN

The resonators in a capacitively loaded interdigital filter consist of an array of coupled-line elements, each having a short circuit to ground at one end and a loading capacitance to ground at the other end. The positions of the short circuits and the loading capacitances alternate from one resonator to the next, as shown in Fig. V-1. For the particular configuration considered here, the short circuits on the first and last resonators are replaced by the terminating admittances. Design equations

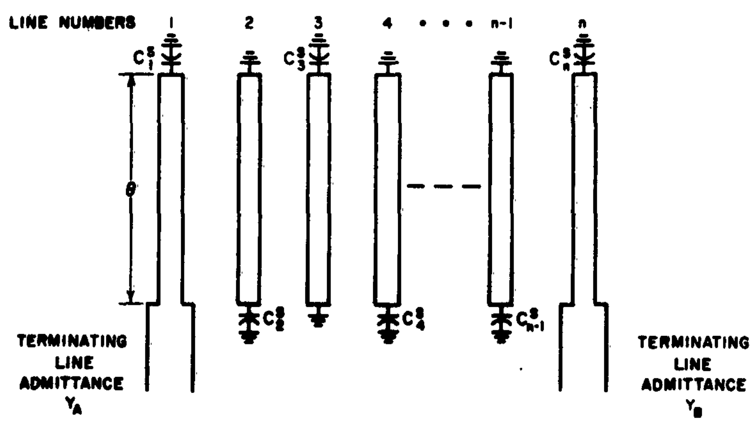

FIG. V-1 CAPACITIVELY LOADED INTERDIGITAL FILTER WITH UNGROUNDED END RESONATORS

and calculated frequency responses for wide-band, band-pass filters of the type illustrated in Fig. V-1 were presented in a previous report.[1*] A capacitively loaded interdigital filter has been constructed for the dual purposes of experimentally confirming the predicted performance and of introducing a printed-circuit-construction technique that may prove useful in production of filters using coupled-line elements.

* References for Sec. V are grouped at the end of the section.

This experimental filter is based on one of the designs presented previously, along with its calculated frequency response.[1] The design parameters, center frequency, and physical dimensions closely parallel those of an interdigital filter previously constructed without capacitive loading.[2] The design is derived from a low-pass prototype with eight reactive elements and Chebyshev response with 0.1-db ripples. The filter dimensions were calculated as outlined in Secs. VI-C and VI-D of Ref. 1. The coupled-line elements were chosen $\lambda/8$ long at the resonance frequency ω_0, so the electrical length at ω_0 is $\theta_0 = \pi/4$. The lower-band-edge frequency ω_1 was chosen as $0.65\ \omega_0$, which would give 2.08-to-1 bandwidth if the frequency response had arithmetic symmetry about ω_0. Equal terminating admittances $Y_A = Y_B = 0.02$ mho were used. The admittance-scale parameter d was chosen as 0.65, based on the calculated frequency responses presented in Ref. 1. The admittance-scale parameters h_A and h_B were set equal to 0.25 to give convenient widths for the coupled-line elements.*

The above parameters, used with the design equations of Table VI D-1 of Ref. 1, give the capacitances tabulated in the second, fifth, and seventh columns of Table V-1 of the present report. The $C_{1,2}$, $C_{2,3}$ ... $C_{7,8}$ are the mutual capacitances per unit length between adjacent coupled-line elements, and C_1, C_2, ..., C_8 are the self capacitances per unit length from the coupled-line elements to ground. The normalizing factor ϵ is the absolute permittivity of the medium surrounding the coupled-line elements, which is air for this filter. The C_1^s, C_2^s, ..., C_8^s are the loading capacitances shown in Fig. V-1.

From the capacitances in Table V-1, it is possible to find the widths and spacings of the coupled-line elements once the ground-plane spacing and coupled-line thickness have been chosen. A ground-plane spacing of $b = 0.625$ inch was chosen, consistent with the dimensions of the type-N connectors. Rather thin coupled-line elements were used,

*The parameters in Table VI E-3 of Ref. 1, for which $h_A = h_B = 0.18$, gave a negative width for the second element and next-to-last coupled-line element. Changing h-parameters raised the admittance level of the filter so that it could be physically realized. The impedance discussed under Eq. (VI D-1) of Ref. 1 was found to be 51 ohms, which is somewhat lower than the 70-ohm value thought to be optimum to minimize dissipation loss. As will be shown, however, the actual filter had reasonably low dissipation loss.

Table V-1

DIMENSIONS AND DESIGN PARAMETERS OF EXPERIMENTAL CAPACITIVELY LOADED INTERDIGITAL FILTER

k	$\frac{C_{k,k+1}}{\epsilon}$	$s_{k,k+1}$ (inches)	k	$\frac{C_k}{\epsilon}$	w_k (inches)	C_k^s (pf)	ℓ_k (inches)
1 and 7	1.664	0.055*	1 and 8	1.664	0.095†	0.90	0.376§
2 and 6	1.249	0.086	2 and 7	0.996	0.105†	0.83	0.316△
3 and 5	1.348	0.077	3 and 6	1.988	0.224	1.23	0.252
4	1.333	0.078	4 and 5	1.984	0.226	1.26	0.254

where

$\theta_0 = \pi/4$ = Electrical length of coupled-line elements at resonance

$\omega_1/\omega_0 = 0.65$ = Ratio of lower band edge to resonance frequencies

$h_A = h_B = 0.25$, $d = 0.65$ = Admittance scale factors

$Y_A = Y_B = 0.02$ mho = Terminating admittances

$L = 0.940$ inch = Length of coupled-line elements

$f_0 = 1.57$ Gc = Design value of resonance frequency

$b = 0.625$ inch = Ground plane spacing over coupled-line elements

$b' = 0.084$ inch = Ground plane spacing over capacitive-loading tabs

$t = 0.024$ inch = Thickness of coupled-line elements

$s_{k,k+1}$ = Spacing between kth and $(k+1)$th coupled-line elements

w_k = Width of kth coupled-line element

ℓ_k = Length of capacitive-loading tab on the kth coupled-line element

* Changed to 0.040 inch during tune-up procedure.

† Width correction[3] for narrow strips used.

§ Shortened 0.10 inch during tune-up procedure.

△ Shortened 0.05 inch during tune-up procedure.

since one objective was to demonstrate a printed-circuit-construction technique for filters such as interdigital and comb-line filters. In this construction technique, each coupled-line element consists of two thin copper strips of equal width, one on each side of a sheet of dielectric. The dielectric sheet provides mechanical support for the thin copper strips. In the gap between adjacent coupled-line elements, the dielectric sheet is removed by machining or punching so that all modes within the filter propagate at free-space velocity. Certain of the design curves,[3] however, are available only for coupled-line elements that are of solid metal. In order to be able to use the available design curves without introducing significant errors, the thickness of the coupled-line elements was chosen small compared to both widths and spacings of the coupled-line elements. An available sheet of copper-clad dielectric of total thickness t = 0.024 inch was used in this particular filter. Having fixed the ground-plane spacing and the coupled-line thickness, the coupled-line widths and spacings were found as outlined in Sec. VI-C of Ref. 1. These dimensions are shown in the third and sixth columns of Table V-1.

The type of loading capacitances used with this filter is illustrated in Fig. V-2. One end of each coupled-line element projects into a region where the ground-plane spacing is reduced from a value

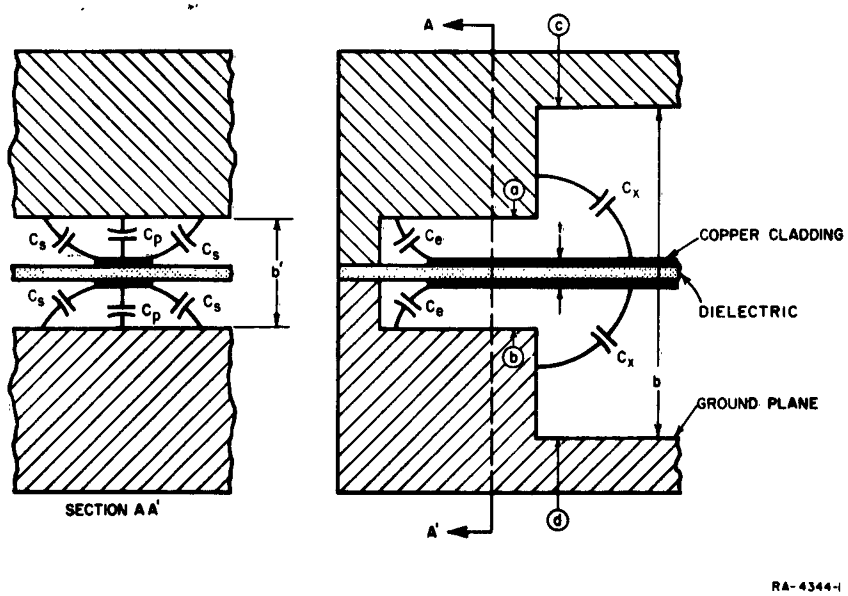

FIG. V-2 TYPE OF LOADING CAPACITANCE USED AT THE END OF EACH COUPLED-LINE ELEMENT

b to a value b', where $b' \ll b$. This forms a parallel-plate capacitance, C_p, between each side of the coupled-line element and the ground planes. There also exist, however, significant fringing capacitances, whose values must be estimated. The side fringing capacitances, C_s, and the end fringing capacitances, C_e, can be estimated with fair accuracy using the fringing per unit length from the corners of an isolated solid conductor of thickness t between ground planes spaced b' apart.[3,4] For the fringing capacitance C_x external to the capacitive gap, accurate data do not exist. The approach used to estimate C_x was to start with the data of Whinnery and Jamieson[5] for the capacitance per unit width at a change from height $\frac{1}{2}(b - t)$ to height $\frac{1}{2}(b' - t)$ in parallel-plate transmission line. An estimate for C_x was obtained by multiplying this capacitance per unit width by an effective width that was 20 to 45 percent greater than the actual width of each coupled-line element.

Using the approximations described in the preceding paragraph, it was found that the lengths of the capacitive-loading tabs should be as given in the last column of Table V-1. For these particular dimensions, it is estimated that the parallel-plate capacitance C_p in Fig. V-2 accounts for 60 to 70 percent of each loading capacitance, the side fringing C_s accounts for 13 to 27 percent of the total, the end fringing C_e accounts for about 6 percent of the total, and the external fringing C_x accounts for only about 10 percent of the total. Thus, a rather rough estimate of the external fringing should be sufficient. Because of the approximations involved in designing the loading capacitances, tuning screws were incorporated into the filter. Previous experience had indicated that the tuning would be most critical for the resonators nearest to the filter ends. Thus, tuning screws were provided only for the first and second, and the next-to-last and the last resonators. The tuning screws pass through the ground planes into the capacitive gaps at the points marked *a* and *b* in Fig. V-2.*

The completed filter is shown partially disassembled in Fig. V-3. Arrows indicate the four tuning screws that pass through the top ground plane, and there are four more tuning screws through the bottom ground plane in order to maintain electrical symmetry about a hypothetical plane halfway between the two ground planes. Figure V-3 also shows the coupled-line elements that are copper clad on a sheet of dielectric, which is supported between the ground planes by aluminum blocks. The surfaces of these aluminum blocks are shaped so as to make contact with every other coupled-line element, and to form the loading capacitance for the alternate coupled-line elements. The coupled lines were formed for this particular filter by machining away portions of the copper cladding with an end-mill tool, and by machining away the supporting dielectric between the coupled-line elements. In a production process, the coupled-line elements could be photo etched, and the dielectric between coupled-line elements removed by punching. The terminating coaxial lines are at right angles to the coupled-line elements so that the spacings $s_{1,2}$ and $s_{7,8}$ between end pairs of coupled-line elements

---

* In early tests on the filter, the tuning screws were mounted just outside the capacitive gap at the points marked *c* and *d* in Fig. V-2. For this location of the tuning screws, there was some question as to the influence of the series inductance of the long tuning screws when they approached very close to the resonators. It was found that either location for the tuning screws gave acceptable results. In production models, the tuning screws could probably be omitted once the proper dimensions were found.

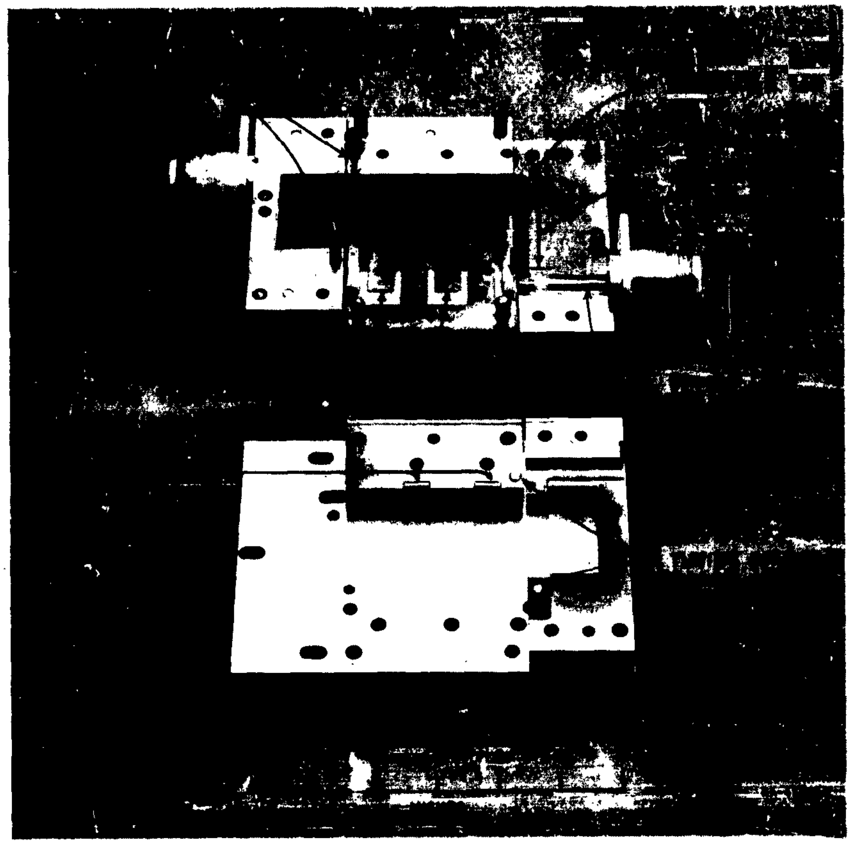

FIG. V-3 PHOTOGRAPH OF THE CAPACITIVELY LOADED INTERDIGITAL FILTER

could be made readily adjustable. Previous experience had indicated the desirability of providing adjustment on these spacings.

B. EXPERIMENTAL RESULTS

Two types of data were taken on the filter shown in Fig. V-3, one being insertion loss as a function of frequency, and the other being reflection coefficient or input VSWR as a function of frequency. Initial measurements for the filter as designed showed that the lowest-frequency ripple in the pass band had an input VSWR of 2.9, which was excessively high, and the remaining three ripples had an input VSWR of about 1.75. Inserting the tuning screws and varying the spacings between end pairs of resonators indicated that the loading capacitances had more capacity than desired. The capacitive tabs on the end coupled-line elements were then shortened as indicated by the footnotes under Table V-1. The procedure used to find the best spacings $s_{1,2}$ and $s_{7,8}$ between end pairs of resonators was to observe the reflection coefficient as sampled using a directional coupler, crystal detector, and oscilloscope while rapidly sweeping the input frequency by means of a backward-wave oscillator. The tuning screws were then varied to obtain the lowest reflection over the pass band, and a record made of the reflection *vs.* frequency. The spacings between end pairs of resonators were then changed, and the tuning procedure repeated. It was found that $s_{1,2}$ and $s_{7,8}$ = 0.040 inch gave the lowest input VSWR over the pass band, although spacings 0.005 inch either side of 0.040 inch gave nearly as good results.

The measured insertion loss as a function of frequency for the filter after final tuning is shown by the crosses and circles in Fig. V-4. The crosses are points read from continuous curves of insertion loss obtained with a logarithmic recorder and a mechanically driven signal generator having leveled output. The circles are directly measured insertion loss taken at discrete frequencies to check the automatic equipment. The solid curve in Fig. V-4 is the calculated frequency response based on the open-wire transmission-line equivalent circuit for the capacitively loaded interdigital filter, (see Fig. VI E-3 of Ref. 1). This calculated curve indicates that the resonance frequency $f_0 = \omega_0/2\pi$, is 5 percent higher than the arithmetic average of the upper and lower band-edge frequencies where the VSWR equals the VSWR of the highest peak in the pass band. Applying this criterion to the measured pass-band VSWR data gives a resonance frequency f_0 = 1.52 Gc, which value was used in normalizing the experimental points plotted in Fig. V-4. This f_0 = 1.52 Gc value is about 3 percent lower than the design value of 1.57 Gc. It is seen that normalization to f_0 = 1.52 Gc gives good agreement between measured and calculated data along the lower edge of the filter response, but the upper edge of the pass band has somewhat narrower bandwidth. This is consistent with the observation made previously (based on the calculated frequency responses),[1] which is that the lower band edge comes out nearly as specified in the design, and the shrinkage in bandwidth occurs at the upper edge of the pass band.*

* In the derivation of the design equations in Ref. 1, the attenuation was specified to be a given value at the resonance frequency, and at the lower band-edge frequency, with no specific control available over the location of the upper band edge.

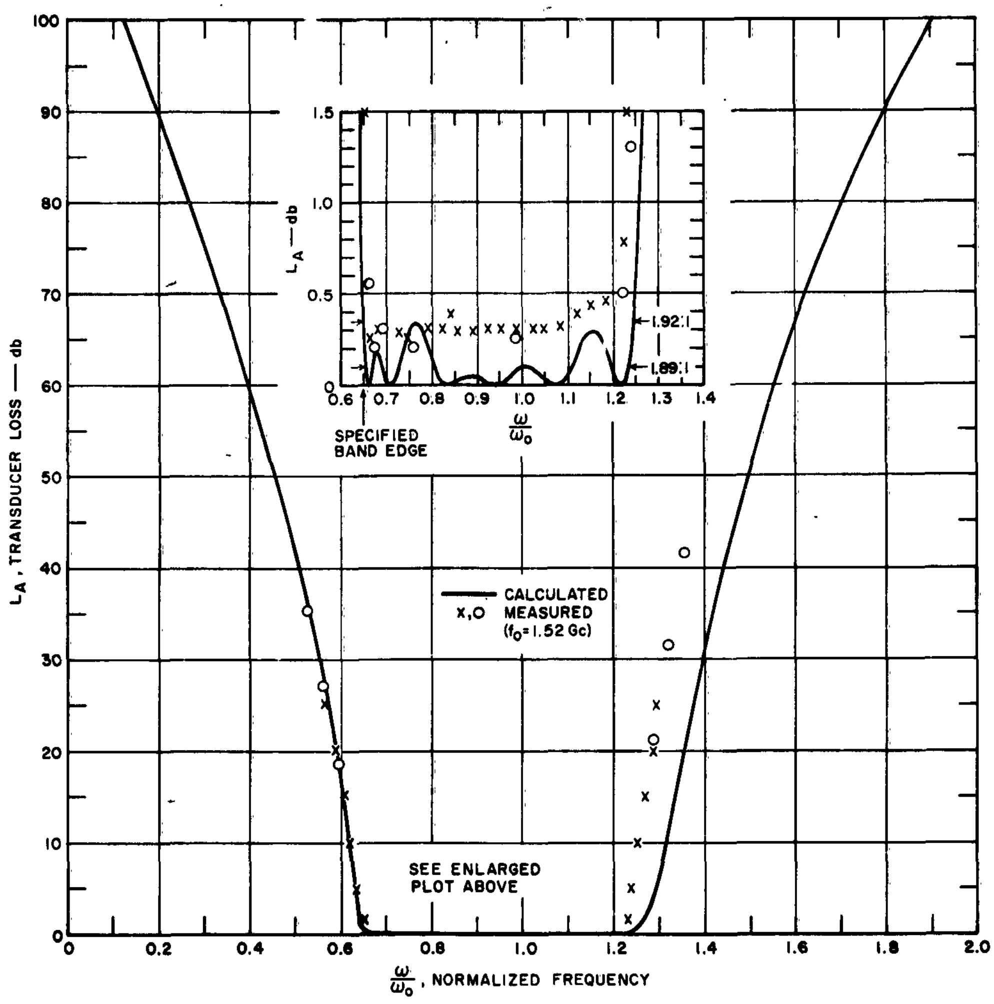

FIG. V-4 MEASURED AND CALCULATED ATTENUATION CHARACTERISTICS OF THE FILTER SHOWN IN FIG. V-3

The insert in Fig. V-4 shows that over most of the pass band, dissipation loss produces an insertion loss of 0.3 db, with the loss rising to 0.5 db at the higher frequencies. Figure V-5 shows that the input VSWR does not exceed 1.35 over the pass band, which means that the loss introduced by power being reflected from the filter input does not exceed 0.1 db. The bandwidth between the frequencies at which the VSWR = 1.35 is 1.85-to-1, as compared to 1.89-to-1 for the calculated frequency response, and as compared to 2.08-to-1 if the frequency response had arithmetic symmetry about f_0.

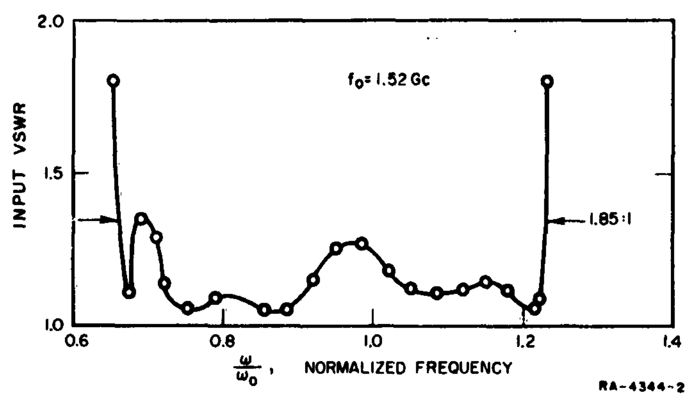

FIG. V-5 MEASURED VSWR OF THE FILTER SHOWN IN FIG. V-3

The second pass band of this filter occurs in the frequency band $4.1 \leq \omega/\omega_0 \leq 4.35$ (centered at 6.7 Gc) and the lowest insertion loss observed in this second pass band was 13 db. This is within the second pass band predicted in Fig. VI E-5 of Ref. 1, but is only about half as wide as predicted. All frequencies between the first and second pass bands were checked with automatic recording equipment whose sensitivity would show any spurious pass bands with less than 45 db insertion loss. No spurious pass bands were observed between the first and second pass bands.

In addition to comparing the measured performance of this filter with its calculated performance, it is of interest to compare this filter with another octave-bandwidth filter that does not have capacitive loading. The predicted advantages of the capacitively loaded interdigital filter over the unloaded interdigital filter are smaller size and greater frequency separation between the first and second pass bands, as was discussed in Sec. VI-A of Ref. 1. These advantages were experimentally confirmed. Other aspects of the measured performance of these two filter types will now also be discussed briefly. Comparing Figs. V-4 and V-5 of this report with Figs. III E-3 and III E-4 of Ref. 2 shows that this particular capacitively loaded filter has slightly lower VSWR over the pass band, but slightly higher average insertion loss over the pass band than does the particular unloaded filter in Ref. 2. The most significant difference, however, is the somewhat narrower pass band of the capacitively loaded filter, which is 1.85-to-1 as compared to 1.95-to-1 for the unloaded filter. Thus, the advantages of smaller size and wider stop band obtained by the use of capacitive loading are paid for by some loss in control of the size of the pass band. With experience, however, it should be possible to design the capacitively loaded interdigital filters to have any desired bandwidth.

A practical matter that requires careful attention when the printed-circuit type coupled-line elements are used is symmetry about a hypothetical plane halfway between the two ground planes. The effects of asymmetry of the tuning screws about this plane were observed in both the reflection coefficient and attenuation curves while tuning up the filter. When one of the tuning screws approached slightly closer to a resonator than did the tuning screw approaching the same resonator from the other side, a narrow-band, S-shaped perturbation would be superimposed on the normal reflection *vs.* frequency curve. When the insertion loss was measured under these conditions, a narrow-band region of high dissipation loss was observed over the same frequency band as the S-shaped perturbation in reflection coefficient.* This effect was particularly sensitive to asymmetry of the tuning screws over the first and last resonators.

* For example, one S-shaped perturbation had a peak VSWR = 1.6, which gives an insertion loss due to reflection of 0.25 db. The measured insertion loss at the same frequency was 2 db, which was due mostly to dissipation loss.

This narrow-band resonance seen in the reflection coefficient and in the insertion responses is thought to be due to a mode in which there is a potential difference between the two printed copper sheets that make up each coupled-line element. Such a mode would have electric fields within the dielectric sheet that supports the copper strips, and significant dissipation loss would occur in the moderately lossy dielectric, ($\tan \delta = 0.001$, $\epsilon_r = 2.7$).* This explanation is supported by the following experiment. When the two tuning screws over the input resonator are turned in until both make contact with the copper strips, they form a good short circuit, and the input reflection coefficient is near unity over the 1-2 Gc sweep range for which the reflection was observed. If either of the tuning screws is then turned out so that it no longer touches the copper strip, the reflection *vs.* frequency response has a deep dip in it at the same frequency where the S-shaped perturbation was observed while tuning up the filter.

Although this dissipation-producing mode can exist when the printed-circuit construction is used, it need not cause any difficulty, provided symmetry is maintained. Electrical symmetry is readily maintained by watching the reflection *vs.* frequency on an oscilloscope while tuning the filter. The two screws associated with a given resonator are tuned by hand in approximate synchronism, and if an S-shaped perturbation appears on the oscilloscope trace, one screw is turned a little more than the other to eliminate the perturbation. This procedure was followed in the final tuning of the filter in Fig. V-3, and only slight evidence of dissipation loss due to the unwanted mode was observed in the insertion loss *vs.* frequency response. The one experimental point at $\omega/\omega_0 = 0.84$ in Fig. V-4 represents the peak of the narrow-band resonance of the unwanted mode. The insertion loss was 0.4 db at this peak, as compared with 0.3 db at adjacent frequencies.

In summary, the measured performance of this capacitively loaded interdigital filter is essentially as predicted. The input VSWR did not exceed 1.35 over the pass band, which is somewhat better than the

---

* For the modes in which the filter is intended to operate, the two copper strips making up each coupled-line element are at the same potential, and thus approximate a solid metal conductor, and produce no fields within the support dielectric.

the predicted peak VSWR of 1.76. The resonance frequency was three percent lower than the value specified in the design. The bandwidth was slightly less than predicted, being 1.85-to-1 as compared to the calculated 1.89-to-1 at the band edges at which the input VSWR = 1.35. The second pass band was at a frequency over four times the resonance frequency, as predicted, and no spurious pass bands were detected between the first and second pass bands. The following factors probably contribute to the differences between the measured and predicted performance. The coupled-line elements are each of two thin copper strips, rather than of solid metal, which reduces the capacitive coupling between adjacent coupled-line elements. There may be significant coupling beyond adjacent coupled-line elements, which was not taken into account in either the filter design, or in the calculated frequency response. The calculation of the capacitive tab dimensions involved estimates of several fringing capacitances, thus tuning screws were necessary on some of the resonators. The advantages of smaller size and wider stop band gained by the use of capacitive loading of interdigital filters are obtained at the cost of slightly less control over the width of the pass band.

REFERENCES

1. G. L. Matthaei, B. M. Schiffman, E. G. Cristal, and L. A. Robinson, "Microwave Filters and Coupling Structures," Section VI, Final Report, SRI Project 3527, Contract DA 36-039 SC-87398, Stanford Research Institute, Menlo Park, California (February 1963).

2. Leo Young and G. L. Matthaei, "Microwave Filters and Coupling Structures," Section III-E, Quarterly Progress Report 4, SRI Project 3527, Contract DA 36-039 SC-87398, Stanford Research Institute, Menlo Park, California (January 1962).

3. W. J. Getsinger, "Coupled Rectangular Bars Between Parallel Plates," *IRE Trans. PGMTT*-**10**, pp. 65-72 (January 1962).

4. S. B. Cohn, "Problems In Strip Transmission Lines," *IRE Trans. PGMTT*-**3**, pp. 119-126 (March 1955).

5. J. R. Whinnery and H. W. Jamieson, "Equivalent Circuits for Discontinuities In Transmission Lines," *Proc. IRE* **32**, pp. 98-114 (February 1944).

VI CONCLUSIONS

A. MULTIPLEXERS

A technique of designing channel separation units in which each unit consists of a band-pass and a band-stop filter operating in conjunction with each other was shown to have interesting possibilities. If both the band-pass and band-stop filters are designed from maximally flat, singly terminated prototypes with the same number of resonators in both filters, a constant-resistance input impedance can be obtained at all frequencies. Fewer resonators can be used in the band-stop filter than in the band-pass filter, if desired, but at the price of some degradation of performance.

B. MAGNETICALLY TUNABLE BAND-STOP FILTERS

Theory was presented for the design of band-stop filters from low-pass prototypes, and a technique for enhancing the coupling to garnet resonators was outlined. The experimental results were in good agreement with the theory. One difficulty that arose was due to direct coupling between the YIG spheres in band-stop Filter 2. This problem might have been avoided by using a low-pass filter structure, which would have provided more shielding between the resonators.

The techniques described for measuring the linewidth of garnet spheres should be very useful, in that these techniques require no special equipment and the tests can be made by use of a simple attenuation measurement.

C. RESONATORS TUNED BY VARACTOR DIODES

Though resonators tuned by varactor diodes are not very practical for most electronically tunable filter applications, such resonators may find practical use in certain types of phase shifters where only a relatively small amount of tuning range is required. One problem that arises in resonators tuned by varactor diodes is that the unloaded Q of the resonator may vary greatly as the diode is tuned. However, circuit configurations were obtained that can avoid this difficulty.

D. INTERDIGITAL FILTER WITH CAPACITIVELY LOADED RESONATORS

The measured results on the trial interdigital filter with capacitively loaded resonators were in good agreement with the theory. The resulting filter was unusually compact, and had a very broad stop band above the first pass band. The main pass band was centered at about 1.5 Gc, while the second pass band was centered at 6.7 Gc. In between, the attenuation was high, with no spurious responses.

ACKNOWLEDGMENTS

Dr. W. E. Wiebenson prepared the computer programs for the analysis of the multiplexer units.

Mr. York Sato made the tests on the magnetically tunable band-stop filters, and worked out many of the details of the trial designs.

The computer program for computing the response of interdigital filters with capacitively loaded resonators was prepared by Mr. V. H. Sagherian. The tests on the trial interdigital filter with capacitively loaded resonators were made partly by Mr. P. R. Reznek and partly by Mr. York Sato.

PROGRAM FOR THE NEXT INTERVAL

It is anticipated that the work for the next interval will include:

(1) Further work on filters with magnetically tunable garnet resonators;

(2) Further work on multiplexers;

(3) Work on microwave impedance-matching filter networks for the broad-banding of devices;

(4) Work on filters using the circular TE_{01} mode; and

(5) Work on electronically tunable up-converters.

IDENTIFICATION OF KEY TECHNICAL PERSONNEL

	HOURS CHARGED TO PROJECT DURING QUARTER
DR. E. G. CRISTAL *Research Engineer*	165
DR. G. L. MATTHAEI *Manager, Electromagnetic Techniques Laboratory (Project Leader)*	140
MR. L. A. ROBINSON *Senior Research Engineer*	38
MR. B. M. SCHIFFMAN *Senior Research Engineer*	148
MR. D. B. WELLER *Research Engineer*	79

DISTRIBUTION LIST

	NO. OF COPIES
OASD (R&E) ATTN: Technical Library Room 3E1065 The Pentagon Washington 25, D.C.	1
Chief of Research and Development OCS, Department of the Army Washington 25, D.C.	1
Commanding General U.S. Army Materiel Command ATTN: R&D Directorate Washington 25, D.C.	1
Commanding General U.S. Army Electronics Command ATTN: AMSEL-AD Fort Monmouth, New Jersey	1
Director, U.S. Naval Research Laboratory ATTN: Code 2027 Washington 25, D.C.	1
Commander, Aeronautical Systems Division ATTN: ASAPRL Wright-Patterson Air Force Base, Ohio	1
Hq, Electronic Systems Division ATTN: ESAL L. G. Hanscom Field Bedford, Massachusetts	1
Commander, Air Force Cambridge Research Laboratories ATTN: CRO L. G. Hanscom Field Bedford, Massachusetts	1
Commander, Air Force Command & Control Development Division ATTN: CRZC L. G. Hanscom Field Bedford, Massachusetts	1
Commander, Rome Air Development Center ATTN: RAALD Griffiss Air Force Base, New York	1
Commander, Armed Services Technical Information Agency ATTN: TISIA Arlington Hall Station Arlington 12, Virginia	10
Chief, U.S. Army Security Agency Arlington Hall Station Arlington 12, Virginia	2
Deputy President U.S. Army Security Agency Board Arlington Hall Station Arlington 12, Virginia	1

	NO. OF COPIES
Commanding Officer Harry Diamond Laboratories ATTN: Library, Room 211, Building 92 Washintton 25, D.C.	1
Corps of Engineers Liaison Office U.S. Army Electronics Research and Development Laboratory Fort Monmouth, New Jersey	1
AFSC Scientific/Technical Liaison Office U.S. Naval Air Development Center Johnsville, Pennsylvania	1
USAELRDL Liaison Office Rome Air Development Center ATTN: RAOL Griffiss Air Force Base, New York	1
Commanding Officer U.S. Army Electronics Materiel Support Agency ATTN: SELMS-ADJ Fort Monmouth, New Jersey	1
Marine Corps Liaison Office U.S. Army Electronics Research and Development Laboratory ATTN: SELRA/LNR Fort Monmouth, New Jersey	1
Commanding Officer U.S. Army Electronics Research and Development Laboratory ATTN: Director of Research or Engineering Fort Monmouth, New Jersey	1
Commanding Officer U.S. Army Electronics Research and Development Laboratory ATTN: Technical Documents Center Fort Monmouth, New Jersey	1
Commanding Officer U.S. Army Electronics Research and Development Laboratory ATTN: SELRA/ADJ (FU No. 1) Fort Monmouth, New Jersey	1
Advisory Group on Electron Devices 346 Broadway New York 13, New York	2
Commanding Officer U.S. Army Electronics Research and Development Laboratory ATTN: SELRA/TNR Fort Monmouth, New Jersey (FOR RETRANSMITTAL TO ACCREDITED BRITISH AND CANADIAN GOVERNMENT REPRESENTATIVES)	3

DISTRIBUTION LIST

Addressee	NO. OF COPIES
Commanding General U.S. Army Combat Developments Command ATTN: CDCMR-E Fort Belvoir, Virginia	1
Commanding Officer U.S. Army Combat Developments Command, Communications-Electronics Agency Fort Huachuca, Arizona	1
Director, Fort Monmouth Office U.S. Army Combat Developments Command, Communications-Electronics Agency Building 410 Fort Monmouth, New Jersey	1
AFSC Scientific/Technical Liaison Office U.S. Army Electronics Research and Development Laboratory Fort Monmouth, New Jersey	1
Commanding Officer and Director U.S. Navy Electronics Laboratory San Diego 52, California	1
Mr. R. Duncan Sperry Microwave Electronics Co. Clearwater, Florida	1
Mr. Philip Carter Physical Electronics Lab 2493 Pulgas Avenue E. Palo Alto, California	1
Melabs Library Stanford Industrial Park 3300 Hillview Avenue Palo Alto, California	1
Mr. Sleven Airborne Instruments Lab Deer Park, New York	1
CO, U.S. Army Electronics Research Unit ATTN: SELRU-3 Mountain View, California	1
Stanford Electronics Laboratory ATTN: Applied Electronics Lab Stanford University Stanford, California	1
Convair Pomona, California	1
Dr. Cohn Rantec Corporation Calabasas, California	1
Mr. Corzine Code 4035 U.S. Naval Ordnance Test Station China Lake, California	1
Dr. Kotzebue Watkins-Johnson 3333 Hillview Avenue Stanford Industrial Park Palo Alto, California	1
Dr. Greimsman Polytechnic Institute of Brooklyn Route 110 Farmingdale, L.I., New York	1
Mr. Mogul Loral Electronics Corporation Plant No. 1, 825 Bronx River Rd, New York 72, New York	1
CO, U.S. Army Signal Equipment Support Agency ATTN: SIGMS/SDM Fort Monmouth, New Jersey	1
Mr. Gustave Shapiro Chief, Engrg. Electronics Section National Bureau of Standards Washington 25, D.C.	1
Chief, Bureau of Ships ATTN: Mr. Gumina, Code 68182 Department of the Navy Washington 25, D.C.	1
Commander, Rome Air Development Center ATTN: Mr. Romanelli, RCLRA-2 Griffiss Air Force Base, New York	1
CO, USAELRDL, ATTN: SELRA/PRM Mr. J. Carter Fort Monmouth, New Jersey	1
CO, USAELRDL, ATTN: SELRA/PEM Mr. Lipetz Fort Monmouth, New Jersey	1
CO, USAELRDL, ATTN: SELRA/PEM Dr. Bady Fort Monmouth, New Jersey	1
CO, USAELRDL, ATTN: SELRA/PEM Mr. W. Dattilo Fort Monmouth, New Jersey	10
CO, USAELRDL, ATTN: SELRA/SEA Mr. B. Ellis Fort Monmouth, New Jersey	1

AD
STANFORD RESEARCH INSTITUTE, Menlo Park, California

NOVEL MICROWAVE FILTER DESIGN TECHNIQUES by G. L. Matthaei, E. G. Cristal, L. A. Robinson, and B. M. Schiffman, Report 1, First Quarterly Progress Report, 1 January to 31 March 1963, 80 pages, 34 Figs., 6 Tables.
Contract DA 36-039-AMC-00084(E)

The results of a mathematical study of a proposed multiplexer design technique are presented. A separate channel unit is used for each channel to be separated out; each unit consists of a band-stop and a band-pass filter. It is shown that such units can be designed to have a constant-resistance input impedance; hence, they can be cascaded without interaction effects.

Design techniques for magnetically tunable band-stop filter using ferrimagnetic garnet resonators are considered. Design for prescribed response is outlined. Use of band-stop filter techniques for measuring linewidth of garnet materials is also discussed.

UNCLASSIFIED

1. Microwave structures
2. Contract DA 36-039-AMC-00084(E)
3. Band-stop filters
4. Tunable filters

UNITERMS

electronic
microwave
multiplexer
band-stop
band-pass
tunable

AD
STANFORD RESEARCH INSTITUTE, Menlo Park, California

NOVEL MICROWAVE FILTER DESIGN TECHNIQUES by G. L. Matthaei, E. G. Cristal, L. A. Robinson, and B. M. Schiffman, Report 1, First Quarterly Progress Report, 1 January to 31 March 1963, 80 pages, 34 Figs., 6 Tables.
Contract DA 36-039-AMC-00084(E)

The results of a mathematical study of a proposed multiplexer design technique are presented. A separate channel unit is used for each channel to be separated out; each unit consists of a band-stop and a band-pass filter. It is shown that such units can be designed to have a constant-resistance input impedance; hence, they can be cascaded without interaction effects.

Design techniques for magnetically tunable band-stop filter using ferrimagnetic garnet resonators are considered. Design for prescribed response is outlined. Use of band-stop filter techniques for measuring linewidth of garnet materials is also discussed.

UNCLASSIFIED

1. Microwave structures
2. Contract DA 36-039-AMC-00084(E)
3. Band-stop filters
4. Tunable filters

UNITERMS

electronic
microwave
multiplexer
band-stop
band-pass
tunable

AD
STANFORD RESEARCH INSTITUTE, Menlo Park, California

NOVEL MICROWAVE FILTER DESIGN TECHNIQUES by G. L. Matthaei, E. G. Cristal, L. A. Robinson, and B. M. Schiffman, Report 1, First Quarterly Progress Report, 1 January to 31 March 1963, 80 pages, 34 Figs., 6 Tables.
Contract DA 36-039-AMC-00084(E)

The results of a mathematical study of a proposed multiplexer design technique are presented. A separate channel unit is used for each channel to be separated out; each unit consists of a band-stop and a band-pass filter. It is shown that such units can be designed to have a constant-resistance input impedance; hence, they can be cascaded without interaction effects.

Design techniques for magnetically tunable band-stop filter using ferrimagnetic garnet resonators are considered. Design for prescribed response is outlined. Use of band-stop filter techniques for measuring linewidth of garnet materials is also discussed.

UNCLASSIFIED

1. Microwave structures
2. Contract DA 36-039-AMC-00084(E)
3. Band-stop filters
4. Tunable filters

UNITERMS

electronic
microwave
multiplexer
band-stop
band-pass
tunable

AD
STANFORD RESEARCH INSTITUTE, Menlo Park, California

NOVEL MICROWAVE FILTER DESIGN TECHNIQUES by G. L. Matthaei, E. G. Cristal, L. A. Robinson, and B. M. Schiffman, Report 1, First Quarterly Progress Report, 1 January to 31 March 1963, 80 pages, 34 Figs., 6 Tables.
Contract DA 36-039-AMC-00084(E)

The results of a mathematical study of a proposed multiplexer design technique are presented. A separate channel unit is used for each channel to be separated out; each unit consists of a band-stop and a band-pass filter. It is shown that such units can be designed to have a constant-resistance input impedance; hence, they can be cascaded without interaction effects.

Design techniques for magnetically tunable band-stop filter using ferrimagnetic garnet resonators are considered. Design for prescribed response is outlined. Use of band-stop filter techniques for measuring linewidth of garnet materials is also discussed.

UNCLASSIFIED

1. Microwave structures
2. Contract DA 36-039-AMC-00084(E)
3. Band-stop filters
4. Tunable filters

UNITERMS

electronic
microwave
multiplexer
band-stop
band-pass
tunable

The use of varactor diodes for tuning transmission line resonators for a proposed form of band-pass-filter phase shifter is discussed. Means are discussed for avoiding excessive variation in resonator Q as the resonator is tuned.

Experimental results are reported from a trial interdigital filter with capacitively loaded resonators. The filter was designed to have a bandwidth of about one octave centered at about 1.5 Gc, a very broad upper stop band, and small physical size. The performance was in good agreement with the theory.

ferrimagnetic
garnet
resonator
linewidth
varactor
filter
interdigital

The use of varactor diodes for tuning transmission line resonators for a proposed form of band-pass-filter phase shifter is discussed. Means are discussed for avoiding excessive variation in resonator Q as the resonator is tuned.

Experimental results are reported from a trial interdigital filter with capacitively loaded resonators. The filter was designed to have a bandwidth of about one octave centered at about 1.5 Gc, a very broad upper stop band, and small physical size. The performance was in good agreement with the theory.

ferrimagnetic
garnet
resonator
linewidth
varactor
filter
interdigital

The use of varactor diodes for tuning transmission line resonators for a proposed form of band-pass-filter phase shifter is discussed. Means are discussed for avoiding excessive variation in resonator Q as the resonator is tuned.

Experimental results are reported from a trial interdigital filter with capacitively loaded resonators. The filter was designed to have a bandwidth of about one octave centered at about 1.5 Gc, a very broad upper stop band, and small physical size. The performance was in good agreement with the theory.

ferrimagnetic
garnet
resonator
linewidth
varactor
filter
interdigital

The use of varactor diodes for tuning transmission line resonators for a proposed form of band-pass-filter phase shifter is discussed. Means are discussed for avoiding excessive variation in resonator Q as the resonator is tuned.

Experimental results are reported from a trial interdigital filter with capacitively loaded resonators. The filter was designed to have a bandwidth of about one octave centered at about 1.5 Gc, a very broad upper stop band, and small physical size. The performance was in good agreement with the theory.

ferrimagnetic
garnet
resonator
linewidth
varactor
filter
interdigital

STANFORD
RESEARCH
INSTITUTE

MENLO PARK
CALIFORNIA

Regional Offices and Laboratories

Southern California Laboratories
820 Mission Street
South Pasadena, California

Washington Office
808 17th Street, N.W.
Washington 6, D.C.

New York Office
270 Park Avenue, Room 1770
New York 17, New York

Detroit Office
1025 East Maple Road
Birmingham, Michigan

European Office
Pelikanstrasse 37
Zurich 1, Switzerland

Japan Office
911 Iino Building
22, 2-chome, Uchisaiwai-cho, Chiyoda-ku
Tokyo, Japan

Representatives

Honolulu, Hawaii
1 25 Ala Moana Blvd.
Honolulu, Hawaii

London, England
19, Upper Brook Street
London, W. 1, England

Milan, Italy
Via Macedonio Melloni, 49
Milano, Italy

Toronto, Ontario, Canada
Room 710, 67 Yonge St.
Toronto, Ontario, Canada